ISSN 2410-3950

Volume 8, Issue 25 – July – December - 2021

Journal of Experimental Systems

ECORFAN®

Journal of Experimental Systems, Volume 8, Issue 25, July – December 2021, is a journal edited sixmonthly by ECORFAN-Bolivia. Loa 1179, Cd. Sucre. Chuquisaca, Bolivia. WEB: www.ecorfan.org/bolivia, journal@ecorfan.org. Editor in Chief: VALDIVIA - BARRERO-ROSALES, José Luis. PhD. ISSN On line: 2410-3950. Responsible for the latest update of this number ECORFAN Computer Unit. ESCAMILLA-BOUCHÁN, Imelda. PhD, LUNA-SOTO, Vladimir. PhD, last updated December 31, 2021.

Journal of Experimental Systems

Definition of Research Journal

Scientific Objectives

Support the international scientific community in its written production Science, Technology and Innovation in the Field of Biology and Chemistry, in Subdisciplines Logical Methods, Research methods, Hypothetical-deductive method, Scientific observation method, Measuring method, Scientific experimentation, Climatology, Geology, Geochemistry, Acoustics.

ECORFAN-Mexico SC is a Scientific and Technological Company in contribution to the Human Resource training focused on the continuity in the critical analysis of International Research and is attached to CONACYT-RENIECYT number 1702902, its commitment is to disseminate research and contributions of the International Scientific Community, academic institutions, agencies and entities of the public and private sectors and contribute to the linking of researchers who carry out scientific activities, technological developments and training of specialized human resources with governments, companies and social organizations.

Encourage the interlocution of the International Scientific Community with other Study Centers in Mexico and abroad and promote a wide incorporation of academics, specialists and researchers to the publication in Science Structures of Autonomous Universities - State Public Universities - Federal IES - Polytechnic Universities - Technological Universities - Federal Technological Institutes - Normal Schools - Decentralized Technological Institutes - Intercultural Universities - S & T Councils - CONACYT Research Centers.

Scope, Coverage and Audience

Journal of Experimental Systems is a Research Journal edited by ECORFAN-Mexico S.C in its Holding with repository in Bolivia, is a scientific publication arbitrated and indexed with semester periods. It supports a wide range of contents that are evaluated by academic peers by the Double-Blind method, around subjects related to the theory and practice Logical Methods, Research methods, Hypothetical-deductive method, Scientific observation method, Measuring method, Scientific experimentation, Climatology, Geology, Geochemistry, Acoustics with diverse approaches and perspectives , That contribute to the diffusion of the development of Science Technology and Innovation that allow the arguments related to the decision making and influence in the formulation of international policies in the Field of Biology and Chemistry. The editorial horizon of ECORFAN-Mexico® extends beyond the academy and integrates other segments of research and analysis outside the scope, as long as they meet the requirements of rigorous argumentative and scientific, as well as addressing issues of general and current interest of the International Scientific Society.

Editorial Board

Arbitration Committee

Assignment of Rights

The sending of an Article to Journal of Experimental Systems emanates the commitment of the author not to submit it simultaneously to the consideration of other series publications for it must complement the Originality Format for its Article.

The authors sign the Authorization Format for their Article to be disseminated by means that ECORFAN-Mexico, S.C. In its Holding Bolivia considers pertinent for disclosure and diffusion of its Article its Rights of Work.

Declaration of Authorship

Indicate the Name of Author and Coauthors at most in the participation of the Article and indicate in extensive the Institutional Affiliation indicating the Department.

Identify the Name of Author and Coauthors at most with the CVU Scholarship Number-PNPC or SNI-CONACYT- Indicating the Researcher Level and their Google Scholar Profile to verify their Citation Level and H index.

Identify the Name of Author and Coauthors at most in the Science and Technology Profiles widely accepted by the International Scientific Community ORC ID - Researcher ID Thomson - arXiv Author ID - PubMed Author ID - Open ID respectively.

Indicate the contact for correspondence to the Author (Mail and Telephone) and indicate the Researcher who contributes as the first Author of the Article.

Plagiarism Detection

All Articles will be tested by plagiarism software PLAGSCAN if a plagiarism level is detected Positive will not be sent to arbitration and will be rescinded of the reception of the Article notifying the Authors responsible, claiming that academic plagiarism is criminalized in the Penal Code.

Arbitration Process

All Articles will be evaluated by academic peers by the Double Blind method, the Arbitration Approval is a requirement for the Editorial Board to make a final decision that will be final in all cases. MARVID® is a derivative brand of ECORFAN® specialized in providing the expert evaluators all of them with Doctorate degree and distinction of International Researchers in the respective Councils of Science and Technology the counterpart of CONACYT for the chapters of America-Europe-Asia- Africa and Oceania. The identification of the authorship should only appear on a first removable page, in order to ensure that the Arbitration process is anonymous and covers the following stages: Identification of the Research Journal with its author occupation rate - Identification of Authors and Coauthors - Detection of plagiarism PLAGSCAN - Review of Formats of Authorization and Originality-Allocation to the Editorial Board- Allocation of the pair of Expert Arbitrators-Notification of Arbitration -Declaration of observations to the Author-Verification of Article Modified for Editing-Publication.

Instructions for Scientific, Technological and Innovation Publication

Knowledge Area

The works must be unpublished and refer to topics of Logical Methods, Research methods, Hypothetical-deductive method, Scientific observation method, Measuring method, Scientific experimentation, Climatology, Geology, Geochemistry, Acoustics and other topics related to Biology and Chemistry.

Presentation of Content

In the first article we present, *Elaboration of Octagonal Roses to represent the wind patterns in the Port de Veracruz during the last 10 years*, by GONZALEZ-JUAREZ Aníbal, AGUILAR-RAMIREZ Ana María, UTRERA-ZARATE, Alberto and MOLINA-NAVARRO, Antonio, with adscription in the Instituto Oceanográfico del Pacifico, as next article we present, *Comparative study between Biological treatment and a physicochemical treatment for the removal of Butyl Acetate in industrial residual effluents*, by CARRILLO-CABRERA, Roxana, RODRIGUEZ-MORALES, Jose Alberto, LEDESMA-GARCIA, Janet and AMARO-REYES, Aldo, with adscription in the Universidad Autónoma de Querétaro, as next article we present, *Thermodynamic analysis of a combined gas-steam cycle without and with afterburner*, by CASADOS-LÓPEZ, Edzel Jair, CASADOS-SÁNCHEZ, Alvaro, ESCAMILLA-RODRÍGUEZ, Frumencio and CORTÉZ-DOMÍNGUEZ, Cristóbal, with adscription in the Universidad Veracruzana, as next article we present, *Rupture voltage in mineral oil using the megger OTS 60pb equipment to determine its quality and use in transformers*, by ESCAMILLA-RODRÍGUEZ, Frumencio, LAGUNA-CAMACHO, Juan Rodrigo, RÍOS-HERNÁNDEZ, Sara Anahí and JIMÉNEZ-CRISTÓBAL, Juan Daniel, with adscription in the Universidad Veracruzana.

Content

Article **Journal of Experimental Systems**
December, 2021 Vol.8 No.25 1-12

Effects of color in humans generated by led lighting systems

Efectos del color en seres humanos generados por sistemas de iluminación led

CÓRDOVA-ESCOBEDO, Jesús Fausto†*, MENDOZA-GONZÁLEZ, Felipe, GOMEZ-RODRIGUEZ, Cristian, and CÓRDOVA-MANZO, Jesús Fausto

Universidad Veracruzana, Facultad de Ingeniería región Coatzacoalcos-Minatitlán, México.

ID 1st Author: *Jesús Fausto, Córdova-Escobedo* / **ORC ID**: 0000-0002-7456-6897, **Researcher ID Thomson**: S-6737-2018, **CVU CONACYT ID**: 511561

ID 1st Co-author: *Felipe, Mendoza-González* / **ORC ID**: 0000-0003-1172-6782, **Researcher ID Thomson**: S-6747-2018, **CVU CONACYT ID**: 947336)

ID 2nd Co-author: *Cristian, Gomez-Rodriguez* / **ORC ID**: 0000-0001-9124-6037, **Researcher ID Thomson**: S-6787-2018, **CVU CONACYT ID**: 210208

ID 3rd Co-author: *Jesús Fausto, Córdova-Manzo* / **ORC ID**: 0000-0001-6284-6990, **Researcher ID Thomson**: AAV-9602-2021, **CVU CONACYT ID**: 1149068

DOI: 10.35429/JOES.2021.25.8.1.12 Received July 29, 2021; Accepted November 30, 2021

Abstract

This research evaluates the effects of color in humans generated by LED lighting systems. This evaluation allows us to know the different parameters that these systems generate, such as: the temperature and color of light suitable for human vision and thus be able to implement them in LED lighting designs for work areas. Having an adequate lighting system contributes to visual health and safety by avoiding work accidents. Each color has a different percentage of light reflection and in the same way each color affects us optically and psychologically by causing different sensations and perceptions in human beings such as visual fatigue, exhaustion, eye disorders, lacrimation, irritation, stress, migraines and even impaired vision Taking care of visual health is of vital importance. The methodology for evaluating lighting designs will be with NOM-030-ENER-2012. The contribution of this research will be to know the optimal colors and color temperature of light to use in LED lighting systems and to help lighting system designers in the selection of suitable LEDs and area colors that contribute to the visual health of humans

Led lighting design, Visual Health, Color psychology

Resumen

Esta investigación evalúa los efectos del color en seres humanos generados por sistemas de iluminación led. Esta evaluación permite conocer los diferentes parámetros que generan estos sistemas como son: la temperatura y el color de luz adecuados para la visión humana y así poder implementarlos en diseños de iluminación led para las áreas de trabajo. Contar con un adecuado sistema de iluminación contribuye a la salud visual y seguridad al evitar accidentes de trabajo. Cada color tiene diferente porcentaje de reflexión de la luz y de igual manera cada color nos afecta óptica y psicológicamente al provocar diferentes sensaciones y percepciones en los seres humanos como la fatiga visual, agotamiento, trastornos oculares, lagrimeo, irritación, estrés, Jaquecas e incluso visión alterada. Cuidar la salud visual es de vital importancia. La metodología de evaluación de los diseños de iluminación será con la NOM-030-ENER-2012. La contribución de esta investigación será conocer los colores y temperatura del color de la luz óptimos a usar en sistemas de iluminación led y ayudar a los diseñadores de sistemas de iluminación en la selección de leds adecuado y colores del área que contribuyan a la salud visual de los seres humanos

Diseño de iluminación led, Salud Visual, Psicología del color

Citation: CÓRDOVA-ESCOBEDO, Jesús Fausto, MENDOZA-GONZÁLEZ, Felipe, GOMEZ-RODRIGUEZ, Cristian, and CÓRDOVA-MANZO, Jesús Fausto. Effects of color in humans generated by led lighting systems. Journal of Experimental Systems. 2021. 8-25: 1-12

* Author Correspondence (fcordova@uv.mx).
† Researcher contributing as first author.

Introduction

During the history of man, he has always tried to illuminate his paths, homes, workplaces to see in the dark. In 1962, Nick Holonyak Jr. developed the first visible light LED and mentioned in 1963 that LED lamps would replace incandescent bulbs, he was not wrong since LEDs have a very important role in the modern world and today they are offered in different ways. powers, sizes and shapes, for example, exist in different emission colors (red, purple, blue, green, yellow, orange) and the most popular white and yellow. Its use has increased due to the low power consumption and its long life in hours of approximately 15,000 hours on average.

Currently when designing lighting systems with LEDs, human sensations and perceptions are not always taken into account, which affect human beings in their visual and psychological health, many times only energy saving, resistance to shocks, lights are considered of colors that can be changed by means of an application or command, among others.

Knowing these effects will allow lighting system designers to select the best light color emission with LEDs, respecting the luxes required according to the NOM for study or work areas, and considering the parameters of color temperature, contrast, color rendering quality, glare, color rendering index, generated shadows (dark region where light is obstructed).

These last parameters are often not considered by designers, for example, the shade is used not only to be able to have rest and a state of relaxation at bedtime, but also to carry out normal human activities

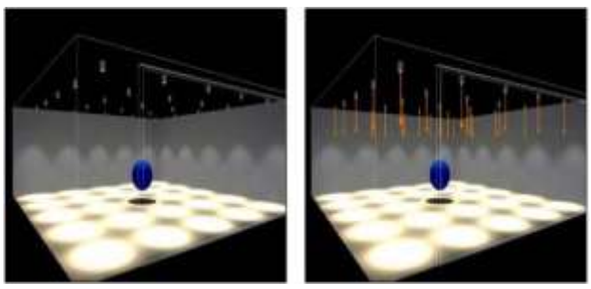

Figure 1 Shadow of a sphere object. White led (left) vs yellow led (right)
Source: Dialux Lighting Manual

Concepts and parameters to consider when designing led lighting

Contrast refers to the phenomenon with which colors can be differentiated according to the brightness and the background color on which it is projected. For sufficiently high levels of illumination, the normal eye is sensitive to colors, while for low levels of illumination the objects are perceived mainly by the contrast of luminances that they present in relation to the background.

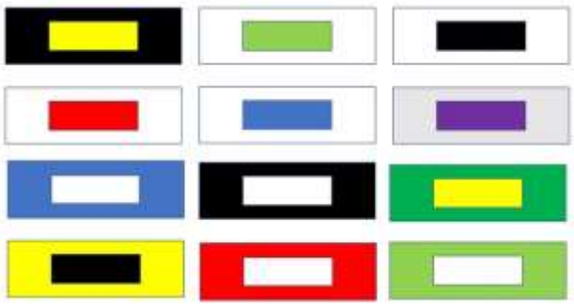

Figure 2 Examples of Contrasts
Source: Own, made in Auto CAD

The difference in luminance between the object being observed and its immediate space is what is known by contrast. The correct combination of colors helps to better distinguish the objects that surround us and thus prevent accidents, the NOM-026-STPS-2008 recommends the following for contrasts:

Safety color	Contrast color
Red	White
Yellow	Black and Magenta
Green	White
Blue	White
Example Reading on monitors	
Black	white

Table 1 Selection of contrasting colors
Source: Secretary of labor and social security

Color measurement

The eye is responsible for color vision, within the retina there are receptors called cones that are sensitive to three wavelengths that correspond to the color red, blue and green, for this reason three numerical components are used to quantify the color. For this reason it is called visual trivariate (RGB system).

ISSN -2410-3950

Chromatic diagram

To avoid that the color evaluations are subjective and can be represented mathematically, systems such as Musell, CIE Lba, CIE y, x, z are used. The Commission Internationale de I'Eclairage defines the CIE Chromatic Diagram as a color identifier, which is used to quantitatively treat light sources, colored surfaces, paints, etc. This diagram represents all the colors that the human eye is capable of seeing. In the diagram, all the colors are ordered by three chromatic coordinates x, y, z, the sum of which is unity.

This means that by having 2 coordinates a color can be defined and by means of the spectral composition the color of the light is determined by calculation. The chromatic diagram, also known as the CIE chromatic triangle, presents a curved shape in the upper part that is where the monochromatic radiations are found, that curve is closed in the lower part by the purple line, which is a straight line . The central part of the triangle is achromatic and the colors of the artificial light sources are located on it. The center is a white point in which the coordinates are equal to each other of 0.333.

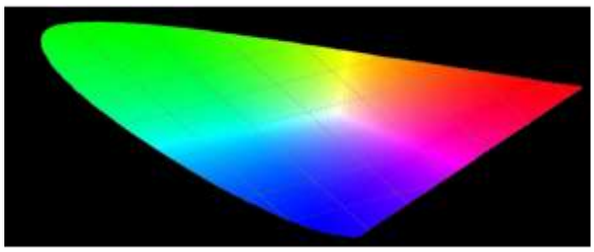

Figure 3 Chromatic diagram
Source: Self Made

The color temperature

Is used to determine how cold or how warm is the light emitted by each led lamp. This measure has a great impact on the area or space that is illuminated. The magnitude of this measure is directly related to the activity carried out in the space to be illuminated. To determine the color temperature of a light source, it is compared with that of a black body, which emits radiation with a wavelength that depends on its temperature. The tone emitted by the luminaire is compared with the tone that the black body has when raising or lowering the temperature. The temperature is assigned to the luminaire when the black body achieves a tone close to the luminaire. If the temperature is low, the tone of the yellow color intensifies.

When the temperature is increased, the blue color intensifies.

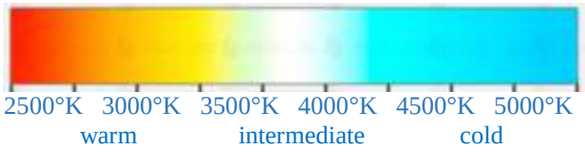

Figure 4 Color temperature
Source: Self Made

Color reproduction

For an object to be appreciated in its entirety, a good color reproduction of said object is needed. The color temperature data refers only to the color of the light, but not to its spectral composition, which is decisive for color reproduction. IRC is defined by its English name Color Rendering Index, as the ability of a source to reproduce the colors of the object it illuminates.

The IRC or RA is independent of the color of the light emitted by the source. A high RA better reproduces the colors of illuminated objects. In order to acquire a good luminaire, you must pay attention to the RA that is indicated on the lamp, which is a numbering that goes after the power, the first digit indicates the IRC, the next two the color temperature. If the number is 870, the 8 means that the lamp has an RA of 80, the number 70 is assigned to the color temperature that means that it has 7000 ° K. The following table shows the quality of the reproduction of the images. colors:

RA	Calidad
RA<60	Poor
60<RA<90	Well
80<RA<90	Very good
90<RA	Excellent

Table 2 Color rendering quality
Source: Self Made

Lamp type RA	Lamp type RA
Incandescent lamps	100
Standard fluorescent lamps	60
Special fluorescent lamps	94
Mercury Vapor Lamps	35-50
Low pressure sodium vapor lamps	20
led lamps	80-95

Table 3 RA for each type of lamp
Source: Self Made

ISSN -2410-3950

Appreciation of objects

Through the contraction of the ciliary muscles, the convexity of the lens of the eye is increased in order to focus on distant or near objects. The process called accommodation (changes in the diameter of the pupil) helps visual focus on the object. When the eye is focused on nearby objects, the pupil contracts slightly and allows less light to enter the eye. On the other hand, when the eye is focused on distant objects, the pupil expands allowing more light to enter. Changes in pupil size are due to three types of reflections: the light reflection, the closeness reflex, and the psycho-sensory reflex.

The light reflection occurs when lighting changes in the environment and the psycho-sensory reflex consists of a pupillary dilation associated with a relevant task or stimulus presented in any sensory modality. In this case the changes in pupil size are more subtle and are mediated by the sympathetic nervous system and are not due to the physical properties of the stimulus but to the cognitive and emotional involvement of the processing. (Duque & Vázquez, 2013).

If the eye works with good lighting, the eye has greater sensitivity at the wavelength of 555 nm in which the greenish-yellow color is found and the minimum of the red and violet colors. The visual field of the human eye is 130 ° vertical and 180 ° horizontal, outside of these angles, the eye does not see any object.

Colors in health

Colors influence our thoughts, emotions and our health. (Graham, 2002). Graham also states in his book, that there have been several studies of the behavior of color in health, one of them is the research of Rudolph Steiner, at the beginning of the 20th century, who related color with figure, shape and sound. He stated that using colors in the correct way, amplifying their color, combination and giving it certain shapes, can become destructive or regenerative for human beings. Today the inspiration of this researcher reaches schools where they are painted and textured according to the stage of development in which the students are.

Researcher Max Lüscher, who was a professor of psychology at the University of Basle, claimed that color shows the state of mind with a physical and psychological diagnosis.

Researcher Robert Gerard proposed that the color red generated anxiety or tension for some people, on the other hand the blue color had a calming effect. Gerald suggested that psychophysiological activation increases with the variation of colors ranging from blue to red, this statement is directly related to the color temperature mentioned here. Gerald, said that blue helped in the treatment of various diseases, as it had therapeutic benefits. He pointed out a clear example such as support for anxious people and support for lowering blood pressure for people with hypertension treatments.

Healing Colors

In 1990, scientists reported at the annual conference of the American Association for the Advancement of Science on the successful use of blue light in the treatment of a wide variety of psychological problems, including addictions, eating disorders, impotence and depression.

Traditional medicine (magic) was used for the same purpose. For example, people with rashes wore red rose petals, those with fever, epilepsy, scarlet fever, and inflammations were dressed in red or had red necklaces. Some of these cases were cured due to the psychological effect produced by beliefs about colors, causing a placebo effect. Another example is:

Pictorial therapy

Considered effective, consists of patients painting situations in their lives with colors that are their favorites or those that they like. With this therapy they help patients to express their feelings through colors and improve their mood.

Glare

According to the Official Mexican Standard NOM-025-STPS-2018 is any glare that causes discomfort and causes interference to vision or visual fatigue. This phenomenon acts on the retina of the eye and produces instability in vision for a short time, after which vision is restored. There are two types of glare, the direct ones, caused by looking directly at the light source: It is the most irritating; as it results in fatigue and reduces perception. The Reflected: It is produced by the incidence of light rays on the object that is observed, such as a metal. If the phenomenon is very prolonged, loss of contrast and visual fatigue occur.

ISSN -2410-3950

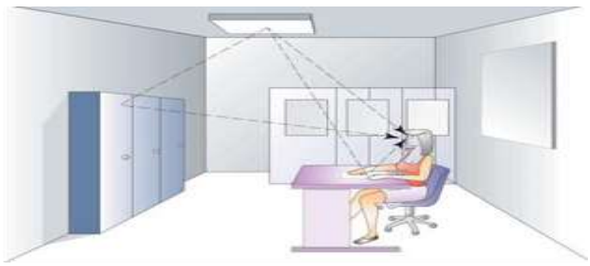

Figure 5 Surfaces causing glare
Source: Luminotecnia. https://rua.ua.es/dspace/pdf

Magnitudes and units of measurement

In lighting technology, magnitudes are used to quantitatively represent the properties of light sources, or the light effects they cause.

Luminous flux

It is the energy of light emitted in all directions by a light source or luminaire per unit of time. Its unit of measurement is the Lumen (lm) and it is represented by the Greek letter Φ. A test is to take two luminaires of different powers, so we could observe that, having different powers, the one with the highest power will provide more light.

Type of lamps	Power	Lm
Incandescent	60W	730
Halogen	1,000W	22,000
sodium vapor	1.000W	120,000
Mercury Vapor	125W	5,600
Fluorescent	65W	5.100
Led	60W	**8,500**

Table 4 Lumens generated by luminaires
Source: Self Made

Luminance

It is the amount of light emitted in a given direction by a luminous or illuminated surface. Its unit of measurement is the candela per surface

Reflection

It is a luminous phenomenon that occurs when a ray of light hits an opaque surface and cannot penetrate, therefore, the ray of light bounces. When light is reflected by a surface, a percentage of that light is lost due to the absorption phenomenon. The relationship between the reflected light and the incident light is called surface reflectance and the surface color is fundamental, for light tones there is greater reflection, for dark tones, there is greater absorption.

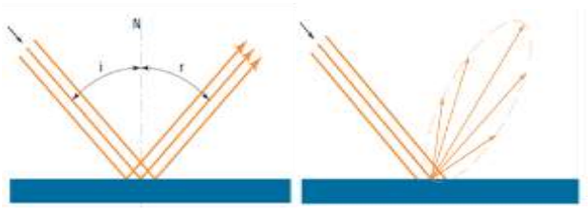

Figure 6 Specular Reflection and Composite Reflection
Source: Luminotecnia. Electrosertec

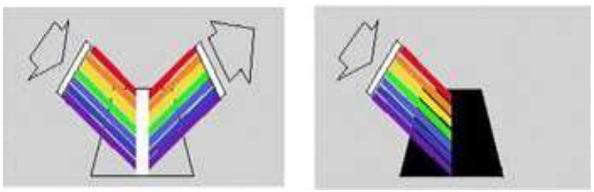

Figure 7 Light absorption
Source: Lighting Manual. https://electrosertec.com

Color psychology

Throughout our lives we live with color, it gives life to objects and our reality. Color in human psychology is the psychoanalysis's term for desires, impulses, and demands. Color has such an influence on human behavior that color speaks to our senses, making us feel different emotions or moods. The effects of color on people range from physiological to psychological, producing different sensations and emotions, therefore, it has different perceptions in each person. Color is capable of motivating or containing, it can create happiness or depression. In the physical it is known that it can produce thermal sensations, they can make us feel hot or cold. Throughout history, the human being has assigned emotional or symbolic meaning to each of the colors. Each of these depend on the time and culture, it is difficult to understand outside the context in which they were given. The attributions of colors are not only studied by artists, but also by doctors, scientists, politicians, communicators, etc. (Fuentes, 2015).

Figure 8 Warm and cold colors
Source: http://profedavidduarte.blogspot.com

ISSN -2410-3950

Hot and cold colors are named because of their position in the electromagnetic spectrum. The warm colors are those which correspond to the long waves, with respect to the cold colors, they are in the short waves. Researcher Robert Gerard proposed that the color red generated anxiety or tension for some people, whereas the color blue had a calming effect. Gerald suggested that psychophysiological activation increases with the variation of colors ranging from blue to red (Graham, 2002).

In the world of work, the use of color in machinery, in work areas, in uniforms, can influence the performance of workers, their safety and their emotional state. The recommended colors for machines that must be worked with during a long day are cold and pale, because they do not disturb visually.
Next, it is shown what each color generates in the human being. (Varley, 1982).

Red: The color red symbolizes energy and heat in psychology, it awakens emotions, such as passion and strength. In bright and strong tones, it symbolizes anger, blood, fire and sex. It is used to mark danger zones, giving a meaning of urgency and importance.

Blue: The color blue represents in psychology the opposite of red, while one represents energy, blue represents calm, purity, it can induce sleep. It can be used to symbolize trust, respect, formality.

Yellow: This color symbolizes energy, kindness, warmth and is characterized by its luminosity. It is used to represent light, the sun, nature and for prevention notices. The yellow ones represent intelligence, it is used in children with learning difficulties and in patients who present anger.

Green: Green refers to nature and harmony, representing freshness and tranquility. In medicine it is associated with the locomotor system, due to its intensity it can be used in hospitals, in luxury, quality and extravagance cases.

Orange: This color represents balance, grace, warmth, fun, and vibrancy. It is associated with vitality. It is used in restaurants. It is best used in small items, as it can cause fatigue when used in large quantities.

Violet: It is related to the nervous system, with it you can treat restlessness, anxiety, tumors, as well as menopause. It is related to mysticism and spirituality. It was used to represent luxury, royalty, femininity, and romanticism.

Brown: This color is associated with tranquility and comfort, it is often used to represent good health. It is used to represent wood, earth, autumn, the rustic.

Black and white: Opposite colors, representing darkness and light respectively. White is synonymous with purity, cleanliness, while black represents sadness, unhappiness. They are colors that when combined with others change their characteristics or representations, for example, the combination with the color red, can make it look like a warm or cold color depending on the mixture. The mixture of both results in the gray color, which represents good taste and is very conservative. When mixed with the black color it can appear vitality.

Methodology

To evaluate the effects generated by LED lighting systems, the Official Mexican Standard (NOM) was taken as a basis. for this case:

NOM-025-STPS-2008: Lighting conditions in work centers.

NOM-007-ENER-2014, Energy efficiency in lighting systems in buildings.

NOM-030-ENER-2016, Luminous efficacy of integrated light-emitting diode (led) lamps for general lighting. Limits and testing methods.

NOM-031-ENER-2012, Energy efficiency for luminaires with light-emitting diodes (LEDs) for roads and public outdoor areas. Specifications and test methods.

It was also used:

a. the lumens method
b. the point-by-point method
c. the dialux software, which allows the simulation and design of LED lighting systems.
d. the POV Raytracer program, which helps to render 3D images.

ISSN -2410-3950

e. A lux meter for lux measurements.
f. A smartphone with the lux meter App to measure lux

The dialux software is evaluated and endorsed software that allows you to create professional lighting projects for interiors and exteriors, respecting the NOM standard. This software has an updated database of various luminaires from various manufacturers in the world.

Phase 1. Data analysis

To determine the effects that led lighting systems generate in humans, a new project will be designed, evaluated and simulated based on a multipurpose academic classroom at the Universidad Veracruzana, Coatzacoalcos campus of the Faculty of Engineering, with the following required measurements and parameters:

- Multipurpose classroom
  - Length: 20 m
  - Width: 15
  - Height: 3.5 m.
- Maintenance plan
  - Degradation factor 0.80

  Degrees of reflection:
  - Soil 80%
  - Wall 80%
  - Roof 50%
- Illumination level
  - 300 lux.
- Type of Luminaire
  - 2600lm 86W luminous flux led,
  - Led with luminous flux 5600 lm of 70W
  - correction factor 1.
  - Color of the LEDs to be used
  - White Simulation 1
  - Yellow simulation 2

Phase 2 Data entry

The data entered for the multipurpose classroom simulation project was

Length: 20 m, width: 15, height: 3.5 m.

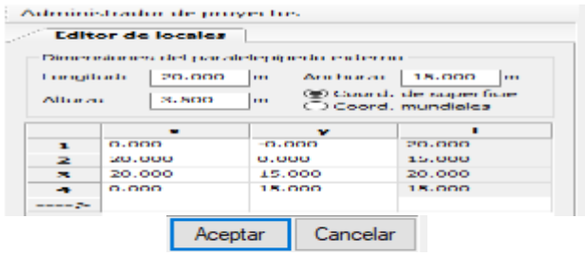

Figure 9 Multiple-use classroom project, data entry. *Source: Dialux Software 4.13*

Subsequently, the maintenance factor of 0.8 is entered, which means that the lighting is in a clean room.

Figure 10 Degradation factor
Source: Obtained from Dialux 4.13

The degree of reflection of the walls, ceiling and floor is entered, they depend on the material with which each of the surfaces and the color. The degrees of reflection that were mentioned will be used.

Degrees of reflection

Floor 20% Wall 80% Ceiling 50%

Figure 11 Degrees of reflection
Source: Dialux 4.13

Classroom object simulation

This simulation allows to determine the possible shadows, contrasts and glare. As the project is a multipurpose classroom with the objects tab, the objects of a classroom with chair, desk, blackboard, windows and doors are placed, where all the objects move and rotate. Colors can be added to all objects. Some texture is added to the doors, walls and windows.

ISSN -2410-3950

Figure 12 3D view of the multipurpose classroom.
Source: Dialux 4.13

Luminaire selection

Subsequently, the luminaire for the premises is selected. There are various catalogs of luminaires, the software in its database has a great variety of luminaires from various manufacturers. For this project, a 2600 luminous flux led luminaire is used, power 86 W, correction factor 1, white color.

Figure 13 Selected luminaire.
Source: Dialux 4.13

Phase 3 Data processing

After entering the data, NOM-025-STPS-2008 determines that the value of the average level of illumination required for a classroom is 300 lx (lux). In the software the average level of illumination required is entered and with this the number of luminaires that are needed to reach the desired level is generated.

Figure 14 Average illumination level 300 lx.
Source: Dialux

Phase 4. Interpretation of the results

Figure 14 shows the result of 9 rows and 5 columns. This indicates that 45 led luminaires with 2600 luminous flux, power 86 W, correction factor 1, white color are required to satisfy the requirements of the 300 lx classroom project. To know the distribution of luminaires, it is calculated by clicking the icon at the top called start calculation.

Phase 5. Validation of the results

The simulation is validated, because it coincides with the results obtained with the lumens method with the same data entered.However, the lumens method calculates 300 lux, with a 7-row x 6-column luminaire distribution variant that results in 42 LED luminaires.Both answers are correct and in this phase, the distribution depends on the designer, in this project is decided by 45 luminaires.

Surface	p [%]	Em[lx]	Emin[lx]	Emax[lx]
Useful Plane	/	309	176	377
Ground	20	286	159	349
The ceiling	80	62	51	96
Walls (4)	50	159	65	327
Useful plan				
Height		0.850 m		
Plot		64 x 64 points		
Marginal zone		0.250 m		

Table 5 Simulation results

The following figure shows the Distribution of the 45 lights of the academic classroom project.

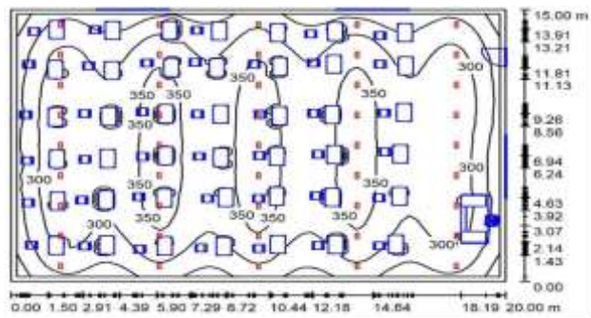

Figure 15 Distribution of the 45 led luminaires and the Isolines generated in the multipurpose classroom.
Source: Dialux 4.13

The simulation results are correct and coincide with those calculated by the lumens method, since the average level of illumination is above that required as determined by NOM-025-STPS-2008 (2008), which in this case is 300 lx. Any professional designer of LED lighting systems would validate this proposal.

ISSN -2410-3950

However, the goal of the research is to offer designers other options such as using yellow LEDs instead of white LEDs.

Phase 6. Simulations with colors

Color influences our personal relationships, moods and our perception of the environment. In the same way, the color emitted by the luminaire affects us. The color of the luminaires generates an effect of tranquility, alteration, heat or cold. Simulations are carried out that will demonstrate which color of the luminaires generates better comfort and helps health, for this simulation the same measurements of the Classroom project will be taken: Length: 20 m, Width: 15 m. Height: 3.5 m, 300 lx,

The luminaire selected for the simulation is:
5600 lm LEDs at 72W

Figure 16 Lamp selection
Source: Dialux 4.13

The same procedure of the first simulation will be followed, with its variants such as the type of luminaire. Different simulations were carried out with different proposals, the results of which are shown in the following figures, source Dialux.

Figure 17 Light colors with yellow light.

Figure 18 Gray colors with white light

Figure 19 Dark colors with white light.

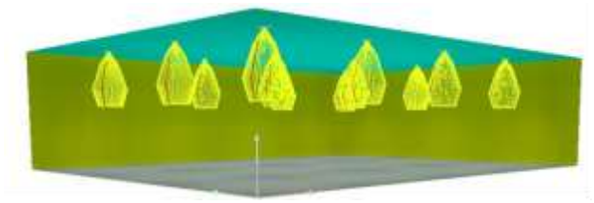

Figure 20 Light colors with yellow light.

Figure 21 Gray colors with yellow light

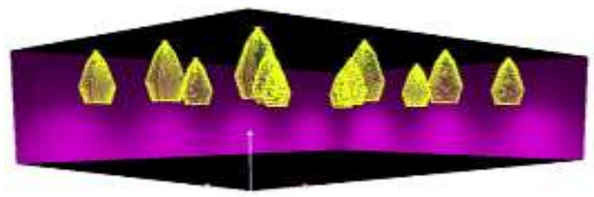

Figure 22 Dark colors with yellow light.

The following table shows the luxes obtained in each simulation grouped by the color of the light.

Type of light	Light colors	Gray colors	Dark colors
Yellow	566 lx	449 lx	363 lx
White	467 lx	431 lx	335 lx

Table 6 Comparison of luxes generated by colors
Source: Self Made

Phase 7. Simulations with color temperatures

The color temperature is modified, for demonstration purposes, luminaires and LEDs are selected with the colorimetric data in which the temperature of the selected luminaire and the spectrum are found. The different color temperatures that were obtained are shown.

ISSN -2410-3950

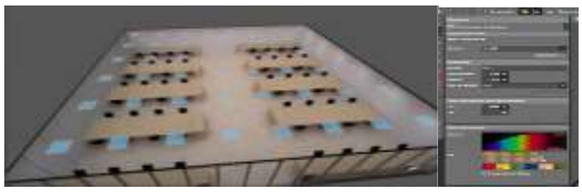

Figure 23 Classroom plan view
Source: Dialux evo

The luminaire selected for the first calculation has a temperature of 4000 ° K. To appreciate the difference in color temperature, three more color temperatures will be selected

Figure 24 4000 ° K data.

Figure 25 Data 25000 °K

Figure 26 Data 6873 °K

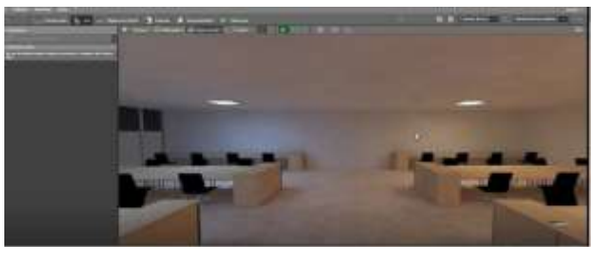

Figure 27 Data 3259 ° K Source: Dialux evo

As can be seen, the color of the light changes with respect to the color temperature of the LED lamp.

Phase 8. Selection of the Light Color for different areas

The colors that are warm are those that are from red to greenish yellow, which is less than 2,700 K and the cold ones are those that go from green to blue and are above 4,000 K, the color of the light will be warmer or cooler depending on how close it is to red or blue, respectively.

The following table shows some recommendations for the light color required to obtain visual comfort:

Area type	Needs	light color
Office, classroom and Mental Health Centers	Comfortable atmosphere clear lighting concentration and do not alter the senses with stress or aggression	Cold light color
Restaurants	Comfort, that is not too intense and relaxing	Warm light color

Table 7 Light color for Classrooms and Restaurants
Source: Self Made

Results

The results of the simulations are correct and coincide with those calculated by the lumens method, since the average level of illumination is above that required as determined by NOM-025-STPS-2008, which in this case is 300 lx In addition, the tables and the blackboard are the most important areas, which have a good level of lighting so there is no need for modification.

The recommended color is cold white led light, a color that generates a perception of cleanliness, calm and spaciousness, ideal for academic activities. It is also advisable to use cool lights, between 4000 and 5000 ° k, because they are the most appropriate to create a work environment that requires looking at short distances and paying close attention. A multipurpose classroom is situated in this context

ISSN -2410-3950

Recommendations

1. Despite the aforementioned benefits of using white light LEDs, it is preferable to use yellow LEDs. The reason is that white light radiates at 2500 ° K or more 60% of the colors visible to the human eye, among this range is the blue color like cell phones. The blue color affects the retina when unprotected eyes look at blue light in the form of a concentrated laser and also suppresses the generation of melatonin causing sleep disorders and as a consequence the quality of life of the patient. Using yellow light LEDs generates less range of blue light in the conditions evaluated in this work.

2. Using light colors for walls, ceilings and floors allows for better lighting due to the percentage of reflection, in addition light colors are relaxing. Dark colors do not help reflection and do not create peace. In the middle of these two extremes, are the gray colors generate feelings of discouragement, they should be used with caution.

3. Consider the psychology of color in the lighting design of the premises, because colors have a great impact on our health and our moods.

4. Avoid lighting systems that generate stroboscopic effects because they give the impression that rotating machines are stopped, which can cause accidents at work.

5. Avoid blue LEDs, because they contribute to damaging the eye macula, related to age with the appearance of cataracts and even blindness.

6. Avoid in lighting designs that the brightness falls directly on the eye. The risk of damage has a lot to do with the power of glitter. LEDs are bright sources of light, if you look at the end, a multicolored image persists on the retina that takes time to disappear.

7. Use endorsed LED lighting system software that comply with the NOM and consider lighting levels, color and light temperature.

Conclusions

Using the lumens method is of utmost importance to design efficient LED lighting systems, because the required lighting levels are guaranteed in lux according to the NOM specifications. Thus, low electricity consumption is achieved. A bad LED lighting design contributes negatively to visual health. An estimated 40 million Mexicans wear glasses.

Normally, in the designs of LED lighting systems, the only aim is to guarantee lighting levels and seek energy savings without considering: The colors of the area to be illuminated, the color temperature of the LEDs and the psychology of color. These contribute to a safe work environment, visual and psychological health and contribute to maximum visual performance, with minimal fatigue.

Poor lighting design leads to dizziness, stress, eye disorders such as sore and swollen eyelids, eyestrain, heaviness, tearing, redness, irritation, even distorted vision, myopia and astigmatism. such as difficulty falling asleep, falling asleep at inappropriate times, abnormal behaviors such as irritability, stress, poor concentration.

It is difficult to establish norms or fixed rules for the correct selection of the color temperature to have a certain effect, for this reason each project has to be treated in a different way due to the diversity of climates and tastes of human sensations such as heat or cold. , in addition to the various activities to be carried out in the areas to be illuminated.

The results obtained with the software simulations are correct and coincide with those calculated by the lumens method, since the average level of illumination is above that required as determined by NOM-025-STPS-2008, which for this case was of 300 lx. The classroom evaluated meets the required luxes, uses white LEDs, has light walls, floors and ceilings, and it is justified to change the white LEDs in the future to yellow LEDs of the same power and luminous flux.

ISSN -2410-3950

References

A. Martínez, C. (1979). psicología del color. plástica/dinámica.

Aguilar Vásquez, A. (2012). Iluminación artificial en viviendas. Universidad del Azuay,

Chapa Carreón, J. (2004). Manual de instalaciones de alumbrado y fotometría. México:

Duque, A., & Vázquez, C. (2013). Implicaciones clínicas del uso del tamaño pupilar como indicador psicológico: una breve revisión. Clínica y salud, 97-100.

Fuentes, F. (2015). psicología del color. Obtenido de scribd: https://es.scribd.com

Garcia Noriega, R. E. (2021). Iluminación con tecnología led para la cancha de fútbol del corregimiento de Cornejo Norte de Santander.

Grados Portocarrero, E. R., Imán Coveñas, J., Melendres Córdova, C. D., Ocaña Huamán, A. R.,& Ojeda Córdova, Y. M. (2021). Análisis económico de tecnologías de iluminación domiciliaria.

Graham, Helen. (2002). Curación con color. Ciudad de México: S.A. Grupo editorial Tomo

Heller, E. (2007). *Psicologia del color*. Munich: Gustavo Gili

Inc. DIAlux. (2020). DIAL. Obtenido de https://www.dial.de/en/dialux

Jean, D. F. (2019). Aplicación de la teoría de los colores de Goethe en la pintura contemporánea de Arequipa. Universidad Nacional de San Agustín de Arequipa, Arequipa.

Jiménez Arévalo, M. (2021). Ecotono. Un sistema de análisis alternativo. Atomósferas desde laluz y el color inmaterial.

Limusa. Ching, F. D. (2012). Diccionario visual de arquitectura. New Jersey: John Wiley y Sons

Mancera Fernandez, M., & Mancera Ruiz , M. T. (2016). Seguridad y salud en el trabajo. Colombia: Alfa omega.

Monteoliva, J., Villalba, A., & Pattini, A. (2015). Temperaturas de color correlacionada de la luz natural: análisis dinámico en espacios interiores. Informes de la construcción, 67(540, 2-8 doi: 10.3989/ic.14.146.

NOM-025-STPS-2008. (2008). Diario oficial de la federación.

Posligua, N., & Castro, M. (2015). Diseño de iluminacion con luminarias tipo led basado en el concepto eficiencia energetica y confort visual; implementacion estructural para pruebas. (Tesis de licenciatura). Universidad Politecnica Salesiana, Guayaquil.

Ruiz Esparza, G., Murieta Cummings, R., Mascott Pérez, Y., Aspe Bernal, M., Rámirez Reyes, R.,& Poon Hung, C. (2015). Manual de iluminación vial. México: Obra independiente.

Secretaria del trabajo y previsión social. (30 de Diciembre de 2008). Diario oficial. Norma Oficial Mexicana NOM-025-STPS-2018. México, México.

Varley Helen & Marshall Editions Ltd (1982). El gran libro del color. España. Editorial Barcelona Blume.

ISSN -2410-3950

Article **Journal of Experimental Systems**
December, 2021 Vol.8 No.25 13-21

Robust linearization scheme by structural state feedback for a quadrotor

Esquema de linealización robusta por realimentación de estado estructural para un cuadricóptero

BLAS-SÁNCHEZ, Luis Ángel†*, GALINDO-MENTLE, Margarita, QUIROZ-RODRÍGUEZ, Adolfo and LICONA-GONZÁLEZ, Marlon

Universidad Tecnológica de Xicotepec de Juárez, Ingeniería en Mantenimiento Industrial, Av. Universidad Tecnológica No. 1000, Col. Tierra Negra, C.P. 73080, Cd. Xicotepec de Juárez, Pue., México

ID 1st Author: *Luis Ángel, Blas-Sánchez* / **ORC ID**: 0000-0003-3313-8551, **Researcher ID Thomson**: AAX-2475-2021, **arXiv Author ID**: AnghelBlas and **CVU CONACYT ID**: 554052

ID 1st Coauthor: *Margarita, Galindo-Mentle* / **ORC ID**: 0000-0001-5390-5960, **Researcher ID Thomson**: S-9202-2018, **arXiv Author ID**: MargaritaG, **CVU CONACYT-ID**: 160164

ID 2nd Coauthor: *Adolfo, Quiroz-Rodríguez* / **ORC ID**: 0000-0002-9685-9455, **Researcher ID Thomson**: S-9189-2018, **arXiv Author ID**: adolfo-79, **CVU CONACYT ID**: 105471

ID 3rd Coauthor: *Marlon, Licona-González* / **ORC ID**: 0000-0001-7829-4457, **Researcher ID Thomson**: AAR-6259-2021, arXiv Author ID marlon1987, **CVU CONACYT-ID**: 1138370

DOI: 10.35429/JOES.2021.25.8.13.21 Received: July 30, 2021; Accepted November 30, 2021

Abstract

In this work a feedback linearization technique is proposed, to carry it out to linearize the dynamic model of the quadrotor, a change of variable is introduced that maps the nonlinearities of the system into a nonlinear uncertainty signal contained in the domain of the action of control and is applied to the dynamic model of the quadrotor. To estimate the nonlinear uncertainty signal, the Beard-Jones filter is used, which is based on standard state observers. To verify the effectiveness of the proposed control scheme, experiments are carried out outdoors to follow a circular trajectory in the (x, y) plane. This presented control scheme is suitable for unmanned aerial vehicles where it is important to reject not only non-linearities but also to seek the simplicity and effectiveness of the control scheme for its implementation.

Linearization, Trajectory tracking, Quadrotor aircraft

Resumen

En este trabajo se presenta una técnica de linealización por realimentación para linealizar el modelo dinámico del cuadricóptero, para llevarla a cabo, se introduce un cambio de variable que mapea las no linealidades del sistema en una señal de incertidumbre no lineal contenida en el dominio de la acción de control y se aplica al modelo dinámico del cuadricóptero. Para estimar la señal de incertidumbre no lineal se utiliza el filtro Beard-Jones, el cual se basa en observadores de estado estándar. Para verificar la efectividad del esquema de control propuesto, se realizan experimentos en exteriores para el seguimiento de una trayectoria circular en el plano (x, y). Este esquema de control presentado es adecuado para vehículos aéreos no tripulados donde es importante rechazar no solo las no linealidades sino también buscar la simplicidad y efectividad del esquema de control para su implementación

Linealización, Seguimiento de trayectoria, Cuadricóptero

Citation: BLAS-SÁNCHEZ, Luis Ángel, GALINDO-MENTLE, Margarita, QUIROZ-RODRÍGUEZ, Adolfo and LICONA-GONZÁLEZ, Marlon. Robust linearization scheme by structural state feedback for a quadrotor. Journal of Experimental Systems. 2021. 8-25: 13-21

* Author Correspondence (luisangel.blas@utxicotepec.edu.mx)
† Researcher contributing as first author.

Introduction

One type of rotary-wing aerial vehicle that has received considerable attention in recent years is quadrotor. These small unmanned helicopters have the capability of vertical takeoff and landing and hovering. Due to their compact size, high maneuverability, and autonomous flight, they have become a standard platform for aerial robotics research around the world.

Unmanned aerial vehicles can be used in many applications such as: earth science, search and rescue, border surveillance, industrial inspection, agriculture, research, etc. This is due to its ease of deployment, low maintenance cost, and hover capability. Unmanned aerial vehicles have been introduced academically as the subject of research projects. The basic dynamic model of the quadrotor is the starting point for all studies carried out. More complete dynamic models have also been obtained by including engine dynamics and aerodynamic effects (Dong et al, 2013), (Hoffmann et al, 2007).

Recently, there has been a great interest in finding simple and effective control schemes for unmanned aerial vehicles (UAVs), capable of rejecting non-linearities and unexpected structure changes. These control schemes must be simple and effective, since they must be programmed in the autopilot incorporated into the quadcopter.

In the literature you can consult the different control techniques that have been evaluated, among them are the Proportional-Derivative (PD) controller (Michael et al, 2010), (Can Dikmen et al, 2009), Proportional-Integral-Derivatice (PID) controller (Bouabdallah et al, 2004), (Li et al, 2011), backstepping controller (Madani et al, 2006), (Huo et al, 2014), non-linear H-infinity controller (V. Raffo et al, 2010), LQR controller (Bouabdallah et al, 2004), sliding modes control and non-linear controllers with nested saturations (Castillo et al, 2005), (Escareno et al, 2006).

A natural and simple control scheme for these non-linear systems is to use the classical Taylor approximation. This is indeed a very simple approach. However, the corresponding techniques must be restricted to a small neighborhood of a fixed reference point.

Under some restrictive assumptions related to external disturbance, this technique can be useful for kinds of regulation problems. On the other hand, it is not recommended, for example, in tracking control problems. Another simple control scheme is the exact input-output linearization technique. This analytical approach requires a complete knowledge of the parameters of the dynamic model, as well as the corresponding derivatives.

Orientation and trajectory tracking control designs based on an inner/outer loop control structure have been presented for normal flight conditions (Li et al, 2010). A robust controller based on the time scale separation approach has been proposed to achieve automatic take-off, hovering, trajectory tracking, and landing missions for a quadcopter (Liu et al, 2014). A state feedback solution is presented to the problem of stabilizing a quadcopter along a predefined trajectory in the presence of constant force disturbances. These disturbances are estimated through the use of adaptive backstepping (Cabecinhas et al, 2014).

A double closed-loop disturbance active rejection control scheme is presented to address some difficult control problems in the quadcopter such as non-linearity, strong coupling, and disturbance sensitivity (Zhang et al, 2018).

This work presents the development and implementation of a control scheme capable of rejecting the non-linearities of the system and compensating for unexpected changes in structure.

Methodology

Dynamic model

To obtain the dynamic model, we consider the quadrotor as a rigid object in three-dimensional space, subjected to a main force and three moments. A rigid body in three-dimensional space has the following generalized coordinates

$$q = \begin{bmatrix} \xi \\ \eta \end{bmatrix} \in \mathbb{R}^6 \quad (1)$$

ISSN 2410-3950

where $\xi = [x \quad y \quad z]^T \in \mathbb{R}^3$ denotes the position vector of the center of mass of the quadrotor relative to the inertial reference frame I. $\eta = [\phi \quad \theta \quad \psi]^T \in \mathbb{R}^3$ expresses the Euler angles with respect to the inertial reference frame, ϕ is the roll angle around the x axis, θ is the pitch angle around the y axis and ψ is the yaw angle around the z axis (García *et al* 2012), (V. Cook, 2013). The positive directions of these angles are chosen according to the right hand rule.

The equations that describe the translational and rotational dynamics are:

$$m\begin{bmatrix} d^2x/dt^2 \\ d^2y/dt^2 \\ d^2z/dt^2 \end{bmatrix} = \begin{bmatrix} u_z(c_\phi s_\theta c_\psi + s_\phi s_\psi) \\ u_z(c_\phi s_\theta s_\psi - s_\phi c_\psi) \\ u_z(c_\phi c_\theta) + mg \end{bmatrix} \quad (2)$$

$$J\ddot{\eta} = \tau - C(\eta, \dot{\eta})\dot{\eta} \quad (3)$$

where m is the mass of the quadcopter, u_z is the main control input or main force applied to the vehicle which is generated by the four rotors, $\tau = [\tau_\phi \quad \tau_\theta \quad \tau_\psi]^T \in \mathbb{R}^3$ represents the roll, pitch and yaw moments, J acts as the inertia matrix for the total rotational kinetic energy of the quadrotor, $C(\eta, \dot{\eta})$ is known as the Coriolis term and contains gyroscopic and centrifugal effects associated with η.

Incremental model

In order to compensate for gravity, the following control law is proposed:

$$u_z = \Delta u_z - mg \quad (4)$$

The expressions of the translational and rotational dynamics are obtained:

$$\begin{bmatrix} d^2x/dt^2 \\ d^2y/dt^2 \\ d^2z/dt^2 \end{bmatrix} = \begin{bmatrix} -\theta g \\ \phi g \\ \frac{1}{m}\Delta u_z \end{bmatrix} + \begin{bmatrix} q_x \\ q_y \\ q_z \end{bmatrix} \quad (5)$$

$$\begin{bmatrix} d^2\phi/dt^2 \\ d^2\theta/dt^2 \\ d^2\psi/dt^2 \end{bmatrix} = \begin{bmatrix} u_y/I_{xx} \\ u_x/I_{yy} \\ u_\psi/I_{zz} \end{bmatrix} + \begin{bmatrix} q_\phi \\ q_\theta \\ q_\psi \end{bmatrix} \quad (6)$$

Where

$$\begin{aligned} q_x &= \theta g - q_{xx} g + \tfrac{1}{m}\Delta u_z q_{xx} \\ q_y &= -\phi g - q_{yy} g + \tfrac{1}{m}\Delta u_z q_{yy} \\ q_z &= -q_{zz} g + \tfrac{1}{m}\Delta u_z q_{zz} \end{aligned} \quad (7)$$

And

$$\begin{aligned} q_{xx} &= c_\phi s_\theta c_\psi + s_\phi s_\psi \\ q_{yy} &= c_\phi s_\theta s_\psi - s_\phi c_\psi \\ q_{zz} &= c_\phi c_\theta \end{aligned} \quad (8)$$

$$\begin{bmatrix} q_\phi \\ q_\theta \\ q_\psi \end{bmatrix} = \left(J^{-1}(\eta) - J^{-1}(0)\right)\tau - J^{-1}(\eta)\, C(\eta, \dot{\eta})\dot{\eta} \quad (9)$$

where q_x, q_y and q_z describe the non-linear part of the translational dynamics, q_ϕ, q_θ and q_ψ describe the non-linear part of the rotational dynamics and $u_y = \tau_\phi$, $u_x = \tau_\theta$ and $u_\psi = \tau_\psi$ are control actions.

State space representations

From equations (5) and (6) the state representations ($i \in \{x, y, z, \psi\}$) are obtained:

$$\frac{d}{dt}\mathrm{x}_i = \mathbf{A}_i \mathrm{x}_i + \mathbf{B}_i u_i + \mathbf{S}_i \mathbf{q}_{oi}, \quad y_i = \mathbf{C}_i \mathrm{x}_i, \quad (10)$$

$$\mathbf{A}_x = \begin{bmatrix} 0 & 1 & 0 & 0 \\ 0 & 0 & -g & 0 \\ 0 & 0 & 0 & 1 \\ 0 & 0 & 0 & 0 \end{bmatrix}, \mathbf{A}_y = \begin{bmatrix} 0 & 1 & 0 & 0 \\ 0 & 0 & g & 0 \\ 0 & 0 & 0 & 1 \\ 0 & 0 & 0 & 0 \end{bmatrix},$$
$$\mathbf{B}_x = I_{yy}^{-1}\boldsymbol{B}_4, \mathbf{B}_y = I_{xx}^{-1}\boldsymbol{B}_4, \mathbf{S}_x = \mathbf{S}_y, \mathbf{C}_x = \mathbf{C}_y,$$
$$\mathbf{B}_4 = \begin{bmatrix} 0 \\ 0 \\ 0 \\ 1 \end{bmatrix}, \mathbf{S}_y = \begin{bmatrix} 0 & 0 \\ 1 & 0 \\ 0 & 0 \\ 0 & 1 \end{bmatrix}, \mathbf{C}_y = \begin{bmatrix} 0 \\ 0 \\ 0 \\ 1 \end{bmatrix}^T \quad (11)$$

$$\mathbf{A}_z = \mathbf{A}_\psi = \begin{bmatrix} 0 & 1 \\ 0 & 0 \end{bmatrix}, \quad \mathbf{B}_z = M_q^{-1}B_2, \quad \mathbf{B}_\psi = I_{zz}^{-1}B_2, \mathbf{S}_z = \mathbf{S}_\psi = \boldsymbol{B}_2, \mathbf{B}_2 = \begin{bmatrix} 0 \\ 1 \end{bmatrix}, \ \mathbf{C}_z = \mathbf{C}_\psi = \begin{bmatrix} 1 \\ 0 \end{bmatrix}^T \quad (12)$$

where $\mathrm{x}_x = \begin{bmatrix} x & dx/dt & \theta & d\theta/dt \end{bmatrix}^T$, $\mathrm{x}_y = \begin{bmatrix} y & dy/dt & \phi & d\phi/dt \end{bmatrix}^T$, $\mathrm{x}_z = \begin{bmatrix} z & dz/dt \end{bmatrix}^T$, $\mathrm{x}_\psi = \begin{bmatrix} \psi & d\psi/dt \end{bmatrix}^T$, $\mathbf{q}_{ox} = \begin{bmatrix} q_x & q_\theta \end{bmatrix}^T$, $\mathbf{q}_{oy} = \begin{bmatrix} q_y & q_\phi \end{bmatrix}^T$, $\boldsymbol{q}_{oz} = q_z$, $\boldsymbol{q}_{o\psi} = q_\psi$. The nonlinear signals q_x, q_y, q_z, q_ϕ, q_θ q_ψ were defined in (7) and (9).

Locally stabilizing feedback

To locally stabilize (10)-(12), the state feedback gain vectors were obtained using the LQR design, that is, the optimal feedback gain matrix is obtained by solving the Riccati algebraic equation:

$$\mathbf{A}_i^T\mathbf{P}_i + \mathbf{P}_i\mathbf{A}_i - \mathbf{P}_i\mathbf{B}_i(\rho_i I)^{-1}\mathbf{B}_i^T\mathbf{P}_i + \mathbf{Q}_i = 0 \quad (13)$$

ISSN 2410-3950

where $i \in \{x, y, z, \psi\}$ and:

$$\mathbf{Q}_x = \mathbf{Q}_y = 900\begin{bmatrix}1 & 0 & 0 & 0\\ 0 & 0 & 0 & 0\\ 0 & 0 & 1 & 0\\ 0 & 0 & 0 & 2.25\end{bmatrix},\ \mathbf{Q}_z = \begin{bmatrix}1 & 0\\ 0 & 0.23\end{bmatrix},\ \mathbf{Q}_\psi = \begin{bmatrix}1 & 0\\ 0 & 0.6\end{bmatrix} \quad (14)$$

$$\rho_x = \rho_y = 1,\ \rho_z = \frac{1}{12100},\ \rho_\psi = \frac{1}{19600} \quad (15)$$

Solving (13) with (11), (12), (14) and (15) for $i \in \{\mathrm{x}, \mathrm{y}, \mathrm{z}, \psi\}$ we obtain for the following state feedbacks:

$$\mathbf{u}_i = \mathbf{F}_i \mathrm{x}_i + \bar{\mathbf{u}}_i,\ i \in \{x, y\} \quad (16)$$

and

$$\mathbf{u}_i = \mathbf{F}_i(\mathrm{x}_i - \bar{\mathrm{x}}_i),\ \ i \in \{z, \psi\}, \quad (17)$$

the optimal state feedback gain vectors:

$$\mathbf{F}_x = \begin{bmatrix}30 & 32.43 & -171.92 & -45.05\end{bmatrix},\ \mathbf{F}_y = \begin{bmatrix}-30 & -32.43 & -171.92 & -45.05\end{bmatrix},\ \mathbf{F}_z = [-140 \quad -69.92],\ \mathbf{F}_\psi = [-110 \quad -85.24] \quad (18)$$

Linearization by structural state feedback

Let's consider the following variable change:

$$\zeta_i = x_i + \mathbf{M}_i \mathbf{C}_{(\mathbf{M}_i, \mathbf{S}_i)} \boldsymbol{\Psi}_n(d^j/dt^j)\, q_{oi}(x, \mathrm{u}) \quad (19)$$

where $\mathbf{C}_{(\mathbf{M}_i, \mathbf{S}_i)} = [S \quad MS \quad \cdots \quad M^{n-1}S]$ and $\boldsymbol{\Psi}_n\left(\frac{d^j}{dt^j}\right) = [\mathrm{I} \quad \mathrm{I}d/dt \quad \cdots \quad \mathrm{I}d^{n-1}/dt^{n-1}]^T$.

State representations (10) feedback with (16) and (18) are written as ($i \in \{x, y\}$):

$$\frac{d}{dt}\zeta_i = \mathbf{A}_{F_i}\zeta_i + \mathbf{B}_i\left(\bar{\boldsymbol{u}}_i + \mathbf{q}_{*i}(\mathbf{x}_i, \mathbf{u}_i)\right),\ \ y_i = \mathbf{C}_i\zeta_i \quad (20)$$

Thus, the exact linearization by structural state feedback is $\bar{\boldsymbol{u}}_i = \mathbf{q}_{*i}(\mathbf{x}_i, \mathbf{u}_i)$, where $\mathbf{A}_{F_i} = \mathbf{A}_i + \mathbf{B}_i\mathbf{F}_i$ and the nonlinear uncertainty signal $\mathbf{q}_{*i}$ is:

$$\mathbf{q}_{*i}(\mathbf{x}_i, \mathbf{u}_i) = \mathbf{X}_i \mathbf{C}_{(\mathbf{M}_i, \mathbf{S}_i)} \boldsymbol{\Psi}_n(d^j/dt^j)\, q_{oi}(\mathbf{x}, \mathbf{u}) \quad (21)$$

where the matrices $\mathbf{M}_i$ and $\mathbf{X}_i$ are solutions of the equation:

$$\mathbf{A}_{F_i}\mathbf{M}_i + \mathbf{B}_i\mathbf{X}_i = \mathrm{I} \quad (22)$$

Nonlinear uncertainty signal estimator

To estimate the nonlinear uncertainty signals, an estimator based on the Beard-Jones filter (V. Beard. 1971), (Bonilla, M. *et al*, 2016) is synthesized for (11):

$$\frac{d}{dt}\mathbf{w}_i = \left(\mathbf{A}_{\mathbf{K}_i} + \mathbf{B}_i\mathbf{G}_i^\ell\mathbf{C}_i\right)\mathbf{w}_i - \left(\mathbf{K}_i + \mathbf{B}_i\mathbf{G}_i^\ell\right)\mathbf{y}_i,$$
$$\bar{\mathbf{u}}_i = \mathbf{G}_i^\ell(\boldsymbol{C}_i\mathbf{w}_i - \mathbf{y}_i) \quad (23)$$

where $\mathbf{A}_{\mathbf{K}_i} = \mathbf{A}_{F_i} + \mathbf{K}_i\mathbf{C}_i$ and $\boldsymbol{G}_i^\ell = -(\boldsymbol{C}_i\boldsymbol{A}_{\mathrm{K}_i}^{-1}\boldsymbol{B}_i)^\ell$ for $i \in \{x, y\}$.

$$\mathbf{A}_{F_i} = \begin{bmatrix}0 & 0 & 0 & -a_{i,4}\\ 1 & 0 & 0 & -a_{i,3}\\ 0 & 1 & 0 & -a_{i,2}\\ 0 & 0 & 1 & -a_{i,1}\end{bmatrix},\ \mathbf{B}_i = \begin{bmatrix}0\\ 0\\ 0\\ -g/I_{yy}\end{bmatrix}, \mathbf{C}_i = \begin{bmatrix}0\\0\\0\\1\end{bmatrix}, \mathbf{K}_i = \begin{bmatrix}a_{i,4} - a_{i_{o,4}}\\ a_{i,3} - a_{i_{o,3}}\\ a_{i,2} - a_{i_{o,2}}\\ a_{i,1} - a_{i_{o,1}}\end{bmatrix}, \quad (24)$$

where $a_{i,1}$, $a_{i,2}$, $a_{i,3}$ and $a_{i,4}$ are the coefficients of the Hurwitz polynomial $\pi_{x_i}(s) = \det(\mathrm{sI} - \mathbf{A}_{F_i}) = s^4 + a_{i,1}s^3 + a_{i,2}s^2 + a_{i,3}s + a_{i,4}$.

The transfer function of the closed-loop system is:

$$\mathrm{F}_{CL}(s) = \mathrm{F}_{\zeta_x}(s)(1 - \mathrm{F}_{e_x}(s)) \quad (25)$$

where

$$\mathrm{F}_{\zeta_i}(s) = \mathbf{C}_i(\mathrm{sI} - \mathbf{A}_{F_i})^{-1}\mathbf{B}_i = \frac{g}{I_{yy}\,\pi_{x_i}(s)} \quad (26)$$

$$1 - \mathrm{F}_{e_x}(s) = 1 - \boldsymbol{G}_i^\ell\mathbf{C}_i\left(\mathrm{sI} - \mathbf{A}_{\mathbf{K}_i}\right)^{-1}\mathbf{B}_i = 1 - \frac{a_{i_{o,4}}}{\pi_{e_i}(s)} = \frac{s\bar{\pi}_{\omega_i}(s)}{\pi_{e_i}(s)} \quad (27)$$

where $\pi_{x_i}(s)$, $\pi_{e_i}(s)$ and $\bar{\pi}_{\omega_i}(s)$ are Hurwitz polynomials.

$$\pi_{e_i}(s) = \det(\mathrm{sI} - \mathbf{A}_{\mathbf{K}_i}) = s^4 + a_{i_{o,1}}s^3 + a_{i_{o,2}}s^2 + a_{i_{o,3}}s + a_{i_{o,4}} \quad (28)$$

$$\bar{\pi}_{\omega_i}(s) = s^3 + a_{i_{o,1}}s^2 + a_{i_{o,2}}s + a_{i_{o,3}} \quad (29)$$

And the polynomials $\pi_{e_i}(s)$ and $\bar{\pi}_{\omega_i}(s)$ are related as follows:

$$\pi_{e_i}(s) = s\bar{\pi}_{\omega_i}(s) + a_{i_{o,4}} \quad (30)$$

Using the root locus procedure, we obtain:

$$\pi_{e_i}(s) = (s+1)(s^2 + 10.25s + 28.125) \quad (31)$$

Scaling the polynomial (31) for $i \in \{x, y\}$ by a positive constant ϱ_{e_x} we obtain:

$$\pi_{e_i}(s) = \left(s + \varrho_{e_x}\right)\left(s^2 + 10.25\varrho_{e_x}s + 28.125{\varrho_{e_x}}^2\right) \quad (32)$$

With $\varrho_{e_x} = 18$ experimentally a good performance was obtained and the polynomial (32) is:

$$\pi_{e_i}(s) = s^4 + 220.5s^3 + 16078.5s^2 + 387828s + 2952450 \quad (33)$$

Drift-free estimator

Experimentally, the nonlinear uncertainty signal estimator (23) performs well when the quadcopter is hovering. However, when we want the quadcopter to follow some trajectory in the (x, y), plane, sometimes the quadcopter exhibits a drift phenomenon.

To overcome the drift we have proceeded as in (P. Gavin, P. *et al*, 1998) and (Horowitz *et al*, 1989), shifting the pole of the origin of (23) slightly to the left of the complex plane. That is, the root of the characteristic polynomial:

$$\pi_{\omega_i}(s) = \det\left(s\mathbf{I}_4 - \left(\mathbf{A}_{\mathbf{K}_i} + \mathbf{B}_i\mathbf{G}_i^{\ell}\mathbf{C}_i\right)\right) = s\bar{\pi}_{\omega_i}(s) = s\left(s^3 + a_{i_{o,1}}s^2 + a_{i_{o,2}}s + a_{i_{o,3}}\right) \quad (34)$$

it is shifted to the left. For this, the parameter $\epsilon a_{i_{o,4}}$ is added, where ϵ is a sufficiently small positive constant. This modification of the characteristic polynomial (34) is achieved by slightly reducing the gain $\boldsymbol{G}_i^{\ell}$ of the nonlinear uncertainty signal estimator (23), that is:

$$\frac{d}{dt}\mathbf{w}_{df,i} = \left(\mathbf{A}_{\mathbf{K}_i} + (1-\epsilon)\mathbf{B}_i\mathbf{G}_i^{\ell}\mathbf{C}_i\right)\mathbf{w}_{df,i} - \left(\mathbf{K}_i + (1-\epsilon)\mathbf{B}_i\mathbf{G}_i^{\ell}\right)\mathbf{y}_i, \quad \bar{\mathbf{u}}_{df,i} = (1-\epsilon)\mathbf{G}_i^{\ell}(\boldsymbol{C}_i\mathbf{w}_{df,i} - \mathbf{y}_i) \quad (35)$$

where $i \in \{x, y\}$.

Notice that the characteristic polynomial of $\mathbf{A}_{\mathbf{K}_i} + (1-\epsilon)\mathbf{B}_i\mathbf{G}_i^{\ell}\mathbf{C}_i$ has no roots at the origin:

$$\pi_{\omega_{df,i}}(s) = \det\left(s\mathbf{I} - \left(\mathbf{A}_{\mathbf{K}_i} + (1-\epsilon)\mathbf{B}_i\mathbf{G}_i^{\ell}\mathbf{C}_i\right)\right)$$
$$\pi_{\omega_{df,i}}(0) = \det\left(\mathbf{A}_{\mathbf{K}_i}\right)\det\left(-1 - (1-\epsilon)\,\mathbf{C}_i\mathbf{A}_{\mathbf{K}_i}^{-1}\mathbf{B}_i\mathbf{G}_i^{\ell}\right) = -\epsilon \neq 0 \quad (36)$$

From (35) and (20), the closed-loop system is:

$$\frac{d}{dt}\begin{bmatrix} e_{df,i} \\ \zeta_i \end{bmatrix} = \mathbf{A}_{CL_{df,i}}\begin{bmatrix} e_{df,i} \\ \zeta_i \end{bmatrix} + \mathbf{B}_{CL_i}\mathbf{q}_{*i},$$
$$\mathbf{y}_i = \mathbf{C}_{CL_i}\begin{bmatrix} e_{df,i} \\ \zeta_i \end{bmatrix} \quad (37)$$

$$\mathbf{A}_{CL_{df,i}} = \begin{bmatrix} \mathbf{A}_{\mathbf{K}_i} & 0 \\ (1-\epsilon)\mathbf{B}_i\mathbf{G}_i^{\ell}\mathbf{C}_i & \mathbf{A}_{\mathbf{F}_i} \end{bmatrix}, \mathbf{B}_{CL_i} = \begin{bmatrix} -\mathbf{B}_i \\ \mathbf{B}_i \end{bmatrix}, \mathbf{C}_{CL_i} = [0 \quad \mathbf{C}_i] \quad (38)$$

where $e_{df,i} = \mathbf{w}_{df,i} - \zeta_i$.

The transfer function of $\Sigma(\mathbf{A}_{CL_{df,i}}, \mathbf{B}_{CL_i}, \mathbf{C}_{CL_i})$ is:

$$\mathrm{F}_{CL_{df,i}}(s) = \mathbf{C}_{CL_i}\left(\mathrm{sI} - \mathbf{A}_{CL_{df,i}}\right)^{-1}\mathbf{B}_{CL_i} = \mathrm{F}_{\zeta_i}(s)(1 - \mathrm{F}_{e_{df,i}}(s)) \quad (39)$$

where:

$$\mathrm{F}_{e_{df,i}}(s) = (1-\epsilon)\mathbf{G}_i^{\ell}\mathbf{C}_i\left(\mathrm{sI} - \mathbf{A}_{\mathbf{K}_i}\right)^{-1}\mathbf{B}_i \quad (40)$$

From (35) and (40) we obtain the polynomials:

$$\pi_{\omega_{df,i}}(s) = \det\left(s\mathbf{I} - \left(\left(\mathbf{A}_{\mathbf{K}_i} + \mathbf{K}_i\mathbf{C}_i\right) + (1-\epsilon)\,\mathbf{B}_i\mathbf{G}_i^{\ell}\mathbf{C}_i\right)\right) = s\bar{\pi}_{\omega_i}(s) + \epsilon a_{i_{o,4}} \quad (41)$$

$$\mathrm{F}_{e_{df,i}}(s) = (1-\epsilon)a_{i_{o,4}}/\pi_{e_i}(s) \quad (42)$$

Trajectory tracking

For the experiments carried out outdoors when the quadrotor follows a circular trajectory of 5 m radius in the (x, y) plane, proceed as follows: the quadcopter is stabilized locally with the LQR and robustly linearized with the drift-free estimators (35), an optimal state trajectory is synthesized to go from a local stationary point to the next local stationary point of the circular trajectory and finally the circular trajectory is partitioned by a finite set of local stationary points.

The local stabilizing feedbacks (16) and the drift-free estimators (35) are written as:

$$\mathbf{u}_i = \mathbf{F}_i(\mathrm{x}_i - \mathrm{x}_i^*) + \bar{\mathbf{u}}_{df,i} \quad (43)$$

$$\frac{d}{dt}\mathbf{w}_{df,i} = \left(\mathbf{A}_{\mathbf{K}_i} + (1-\epsilon)\mathbf{B}_i\mathbf{G}_i^{\ell}\mathbf{C}_i\right)\mathbf{w}_{df,i} - \left(\mathbf{K}_i + (1-\epsilon)\mathbf{B}_i\mathbf{G}_i^{\ell}\right)\boldsymbol{C}_i(\mathrm{x}_i - \mathrm{x}_i^*),\ \bar{\mathbf{u}}_{df,i} = (1-\epsilon)\mathbf{G}_i^{\ell}(\boldsymbol{C}_i\mathbf{w}_{df,i} - \boldsymbol{C}_i(\mathrm{x}_i - \mathrm{x}_i^*)) \quad (44)$$

where $i \in \{x, y\}$ and together with (18) and (24). We want to solve the following control problem, let the linear systems described by the state representations (*cf.* (10), (11), (16) and (18)), consider the linear description in state space:

$$\frac{d}{dt}\mathrm{x}_i^* = \mathbf{A}_{\mathbf{F}_i}\mathrm{x}_i^* + \mathbf{B}_i\bar{\mathbf{u}}_i^*, \qquad i \in \{x, y\} \quad (45)$$

where $\mathbf{A}_{\mathbf{F}_i} = \mathbf{A}_i + \mathbf{B}_i\mathbf{F}_i,\ i \in \{x, y\}$, such that the pairs $(\mathbf{A}_{\mathbf{F}_i}, \mathbf{B}_i)$ are controllable (*cf.* (11)).

Let $\mathrm{x}_i^*(t)$ be a partition of the desired trajectory for $i \in \{x, y\},\ t \in [0, T_f]$ at $N+1$ stationary points, that is:

$$\Lambda_{SP_i}^* = \{\bar{\mathrm{x}}_{0,i}^*, \bar{\mathrm{x}}_{1,i}^*, \bar{\mathrm{x}}_{2,i}^*, \ldots, \bar{\mathrm{x}}_{N,i}^*\},\ \mathrm{x}_i^*(kT_s) = \bar{\mathrm{x}}_{k,i}^* \quad (46)$$

where $k \in \{0, 1, 2, \ldots, N\}$, $NT_s = T_f$ and $i \in \{x, y\}$; T_s is the trajectory sampling time and T_f is the flight time.

We are interested in finding minimum norm control inputs $\bar{\mathbf{u}}_i^*$ such that the solution trajectories, starting from the stationary point $\mathrm{x}_i^*(kT_s) = \mathrm{x}_{k,i}$, reach the next stationary point in finite time, that is: $\mathrm{x}_i^*((k+1)T_s) = \bar{\mathrm{x}}_{(k+1),i}^*$ where T_s is the given sampling time, $T_s > 0$.

This classical minimum norm problem consists of finding the vector closest to the origin that lies in a finite codimension manifold, in a Hilbert space, and is solved with the help of the projection theorem.

According to Theorem 2 of Section 3.3 of (G. Luenberger, 1969), the control input $\bar{\mathbf{u}}_i^*$ to solve the problem has the form:

$$\bar{\mathbf{u}}_i^*(t) = -\mathcal{F}_{F_i}(T_s - t)\mathfrak{W}_{i_{T_s}}^{-1}\exp\left(\boldsymbol{A}_{\boldsymbol{F}_i}T_s\right)\mathrm{x}_{o,i},\ i \in \{\mathrm{x}, \mathrm{y}\}, t \in [0, T_f] \quad (47)$$

Where

$$\mathcal{F}_{F_i} = \mathbf{B}_i^T\exp\left(\mathbf{A}_{\mathbf{F}_i}^T t\right),$$

$$\mathfrak{W}_{i_{T_s}} = \int_0^{T_s}\mathcal{F}_{\boldsymbol{F}_i}^T(T_s - \tau)\mathcal{F}_{\boldsymbol{F}_i}(T_s - \tau)d\tau \quad (48)$$

From (45), (47) and (48) we obtain for all time intervals $[kT_s, (k+1)T_s)$, $k \in \{0, 1, 2, \ldots, (N-1)\}$, the following optimal trajectories:

$$\mathrm{x}_i^*(t) = \exp\left(\boldsymbol{A}_{\boldsymbol{F}_i}(t - kT_s)\right)\bar{\mathrm{x}}_{k,i}^* + \int_{kT_s}^{t}\mathcal{F}_{\mathbf{F}_i}^T(t - \tau)\beta_i^*(t, \tau)v_{k,i}^*d\tau \quad (49)$$

Where

$$\beta_i^*(t, \tau) = \mathcal{F}_{\mathbf{F}_i}(t - \tau)\mathfrak{W}_{i_{T_s}}^{-1},$$
$$v_{k,i}^* = \mathrm{x}_{(k+1),i}^* - \exp\left(\mathbf{A}_{\mathbf{F}_i}T_s\right)\bar{\mathrm{x}}_{k,i}^*,$$
$$\bar{\mathrm{x}}_{k,i}^* = \Lambda_{SP_i}^*, i \in \{\mathrm{x}, \mathrm{y}\} \quad (50)$$

We are interested in following a circular trajectory:

$$\mathrm{x}_*^2(t) + (\mathrm{y}_*(t) - \boldsymbol{r}_*)^2 = \boldsymbol{r}_*^2 \quad (51)$$

this is:

$$\mathrm{x}_*(t) = \boldsymbol{r}_*\sin(\omega_s t)$$
$$\mathrm{y}_*(t) = \boldsymbol{r}_*(1 - \cos(\omega_s t)) \quad (52)$$

where $\omega_s = 2\pi/T_s$. Partitioning T_f in N points we obtain $(t = (k/N)T_s, k \in \{0, 1, 2, \ldots, (N-1)\}$.

$$\left(\bar{x}_{k,x}^*, \bar{x}_{k,y}^*\right) = r_*([\sin(\alpha_k) \quad \omega_s\cos(\alpha_k) \quad \left(\frac{\omega_s^2}{g}\right)\mathrm{sen}(\alpha_k) \quad \left(\frac{\omega_s^3}{g}\right)\cos(\alpha_k)]^T,\ [\left(1 - \cos(\alpha_k)\right) \quad \omega_s\sin(\alpha_k) \quad \left(\frac{\omega_s^2}{g}\right)\cos(\alpha_k) \quad \left(\frac{\omega_s^3}{g}\right)\sin(\alpha_k)]^T) \quad (53)$$

where $\alpha_k = 2\pi k/N$.

Results

Experimental platform

The quadcopter used in the experiments is built on a carbon fiber structure with a length of 498 mm. The Pixhawk flight controller has the following features: a 32-bit STM32F427 Cortex-M4F microprocessor with FPU, 168 MHz, 256 KB of RAM and 2 MB Flash. It has the I2C, PWM interfaces, 5x UART serial ports, two ADC inputs, Spektrum DSM and Futaba inputs.

ISSN 2410-3950

It has the following sensors integrated: magnetometer, barometer, two accelerometers and two gyroscopes. Use an external Ublox Neo-M8N GPS with compass. To power the electronics and motors, LiPo batteries with a capacity of 4000 mAh, three cells and a discharge rate of 45C are used. The quadrotor's propulsion system is composed of four 16-pole 4220-880Kv motors and four 11x4.5-inch propellers.

Figure 1 Quadrotor

Experimental results

The experimental results performed outdoors are presented to follow a circular trajectory tracking of radius $\boldsymbol{r}_* = 5$ m in the (x, y) plane. We consider the following steps: the quadrotor is stabilized locally with the state feedbacks (43) for $i \in \{\mathrm{x}, \mathrm{y}, \psi\}$ and for $i = \mathrm{z}$ we use (17) and (18). The quadcopter is robustly linearized with the drift-free estimators (44) for $i \in \{x, y, \psi\}$ together with (24), (33) and $\epsilon = 1/50$. The circular trajectory for tracking is generated with the help of (48), (49), (50) and (53) with $\boldsymbol{r}_* = 5$ m and $T_s = 1$ s.

A circular trajectory (51) was followed with radius $\boldsymbol{r}_* = 5$ m, sampling time $T_s = 1$s and a partition of $N = 20$ points, that is: $T_s = 20$ s. Graphics 2 to 4 show the results obtained when the locally stabilizing feedbacks (43) are applied with and without the drift free estimators (44). In Graphic 1 the trajectory obtained is compared with the desired circular trajectory. In Graphic 2 the trajectories (x, y) obtained are compared with the reference trajectories. The tracking error $e_c(t)$ is shown in Graphic 3:

$$e_c(t) = \sqrt{(x(t) - x_*(t))^2 + (y(t) - \mathrm{y}_*(t))^2} \quad (54)$$

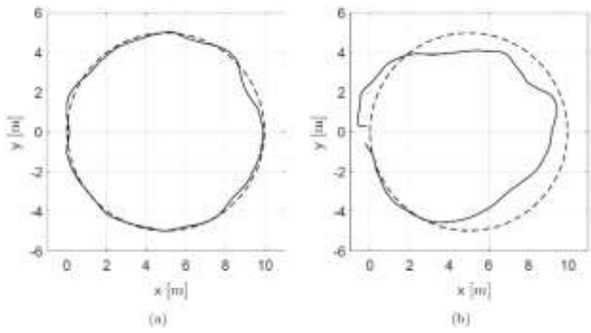

Graphic 1 Circular trajectory tracking in the (x, y) plane with a radius of 5 m in $20\,s$ ($N = 20$ y $T_s = 1$ s). (a) Application of locally stabilizing feedbacks together with drift free estimators. (b) Applying only locally stabilizing feedbacks.

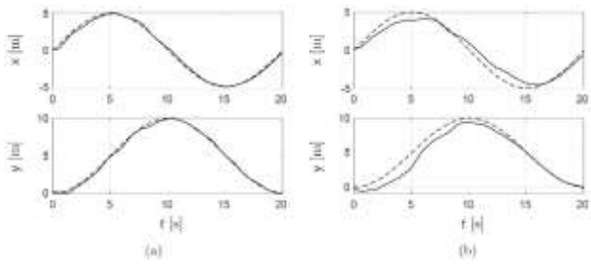

Graphic 2 Comparison of the trajectories in (x, y) with the references. (a) Application of locally stabilizing feedbacks together with drift free estimators. (b) Applying only locally stabilizing feedbacks.

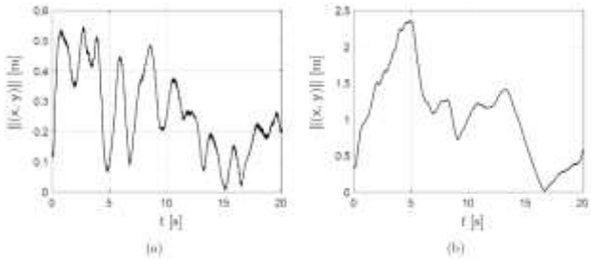

Graphic 3 Comparison of tracking error $e_c(t)$. (a) Application of locally stabilizing feedbacks together with drift free estimators. (b) Applying only locally stabilizing feedbacks.

When the locally stabilizing feedbacks (43) are applied together with the drift free estimators (44), we obtain the maximum error peak $\|e_c\|_p = 0.5463$ m and the mean square error $\|e_c\|_{rms} = 0.2992$ m where:

$$\|e_c\|_p = \max_{t \in [0, T_f]} e_c(t),$$

$$e_c(t) = \sqrt{\frac{1}{T_f} \int_0^{T_f} e_c^2(t) dt} \quad (55)$$

ISSN 2410-3950

When only locally stabilizing feedbacks are applied (43) we obtain the maximum error peak $\|e_c\|_p = 0.9493$ m and the mean square error $\|e_c\|_{rms} = 0.5534$ m.

Conclusions

In this article it was shown that a non-linear system modeled by the state representation (10) can be transformed to the state representation (20). In (10) the non-linearities characterized by the non-linear disturbance signal vector q_{oi}, which acts through S_i. In (20) the nonlinearities are characterized by the non-linear uncertainty signal vector q_{*i}, acting directly through B_i. This transformation is achieved by the change of variable (19), which exists under conditions of torque controllability (A_i, B_i). Since now the nonlinear uncertainty signal q_{*i} (21) acts through B_i, then it can be canceled directly by the control input $\bar{u}_i$.

The exact linearization is based on the analytical reconstruction of q_{*i}; but if this is not possible, it can be estimated. For this, the nonlinear uncertainty signal estimator (23) was proposed based on the Beard-Jones filter, whose objective is to robustly reject the nonlinear uncertainty signal q_{*i}.

Trajectory tracking was addressed and it was found that there is a drift phenomenon when we want the quadcopter to follow some trajectory in the (x, y) plane, to overcome this quadcopter drift phenomenon, it was proposed to shift slightly to the left of the plane complex to the pole at the origin of (23), obtaining the drift free estimator (35).

To circular trajectory tracking in the (x, y) plane, an optimal state trajectory was synthesized (49) and the circular trajectory was partitioned into a finite set of local stationary points (53).

In the outdoor experimental results when the quadcopter follows a circular trajectory of radius 5 m in the (x, y) plane, an appreciable reduction in tracking errors was obtained when applying the drift-free estimators.

References

Dong, W., Gu, G. Y., Zhu, X., & Ding, H. (2013, May). Modeling and control of a quadrotor UAV with aerodynamic concepts. In Proceedings of World Academy of Science, Engineering and Technology (No. 77, p. 437). World Academy of Science, Engineering and Technology (WASET).

Hoffmann, G., Huang, H., Waslander, S., & Tomlin, C. (2007, August). Quadrotor helicopter flight dynamics and control: Theory and experiment. In AIAA guidance, navigation and control conference and exhibit (p. 6461).

Michael, N., Mellinger, D., Lindsey, Q., & Kumar, V. (2010). The grasp multiple micro-uav testbed. IEEE Robotics & Automation Magazine, 17(3), 56-65.

Dikmen, İ. C., Arisoy, A., & Temeltas, H. (2009, June). Attitude control of a quadrotor. In 2009 4th International Conference on Recent Advances in Space Technologies (pp. 722-727). IEEE.

Bouabdallah, S., Noth, A., & Siegwart, R. (2004, September). PID vs LQ control techniques applied to an indoor micro quadrotor. In 2004 IEEE/RSJ International Conference on Intelligent Robots and Systems (IROS)(IEEE Cat. No. 04CH37566) (Vol. 3, pp. 2451-2456). IEEE.

Li, J., & Li, Y. (2011, August). Dynamic analysis and PID control for a quadrotor. In 2011 IEEE International Conference on Mechatronics and Automation (pp. 573-578). IEEE.

Madani, T., & Benallegue, A. (2006, October). Backstepping control for a quadrotor helicopter. In 2006 IEEE/RSJ International Conference on Intelligent Robots and Systems (pp. 3255-3260). IEEE.

Huo, X., Huo, M., & Karimi, H. R. (2014). Attitude stabilization control of a quadrotor UAV by using backstepping approach. Mathematical Problems in Engineering, 2014.

Raffo, G. V., Ortega, M. G., & Rubio, F. R. (2010). An integral predictive/nonlinear H∞ control structure for a quadrotor helicopter. Automatica, 46(1), 29-39.

ISSN 2410-3950

Castillo, P., Lozano, R., & Dzul, A. (2004, September). Stabilization of a mini-rotorcraft having four rotors. In 2004 IEEE/RSJ International Conference on Intelligent Robots and Systems (IROS)(IEEE Cat. No. 04CH37566) (Vol. 3, pp. 2693-2698). IEEE.

Escareno, J., Salazar-Cruz, S., & Lozano, R. (2006, June). Embedded control of a four-rotor UAV. In 2006 American Control Conference (pp. 6-pp). IEEE.

Zhou, Q. L., Zhang, Y., Rabbath, C. A., & Theilliol, D. (2010, October). Design of feedback linearization control and reconfigurable control allocation with application to a quadrotor UAV. In 2010 Conference on Control and Fault-Tolerant Systems (SysTol) (pp. 371-376). IEEE.

Liu, H., Bai, Y., Lu, G., Shi, Z., & Zhong, Y. (2014). Robust tracking control of a quadrotor helicopter. Journal of Intelligent & Robotic Systems, 75(3), 595-608.

Cabecinhas, D., Cunha, R., & Silvestre, C. (2014). A nonlinear quadrotor trajectory tracking controller with disturbance rejection. Control Engineering Practice, 26, 1-10.

Zhang, Y., Chen, Z., Zhang, X., Sun, Q., & Sun, M. (2018). A novel control scheme for quadrotor UAV based upon active disturbance rejection control. Aerospace science and technology, 79, 601-609.

Carrillo, L. R. G., López, A. E. D., Lozano, R., & Pégard, C. (2012). Quad rotorcraft control: vision-based hovering and navigation. Springer Science & Business Media.

Cook, M. V. (2012). Flight dynamics principles: a linear systems approach to aircraft stability and control. Butterworth-Heinemann.

Beard, R. V. (1971). Failure accomodation in linear systems through self-reorganization (Doctoral dissertation, Massachusetts Institute of Technology).

Bonilla, M., Blas, L. A., Salazar, S., Martínez, J. C., & Malabre, M. (2016, June). A robust linear control methodology based on fictitious failure rejection. In 2016 European Control Conference (ECC) (pp. 2596-2601). IEEE.

Gavin, H. P., Morales, R., & Reilly, K. (1998). Drift-free integrators. Review of scientific instruments, 69(5), 2171-2175.

Horowitz, P., Hill, W., & Robinson, I. (1989). The art of electronics (Vol. 2, p. 658). Cambridge: Cambridge university press.

Luenberger, D. G. (1997). Optimization by vector space methods. John Wiley & Sons.

ISSN 2410-3950

Article **Journal of Experimental Systems**
December, 2021 Vol.8 No.25 22-29

Design, construction and testing of a floating hood biodigester prototype for municipal waste organic waste

Diseño, construcción y prueba de prototipo biodigestor de campana flotante para residuos orgánicos de rastro municipal

ACOSTA-PINTOR, Dulce Carolina†*, MOJICA-MESINAS, Cuitláhuac, VIDAL-BECERRA, Eleazar and GONZÁLEZ-ZARAZÚA, Jonathan de Jesús Constantino

Tecnológico Nacional de México – Campus Ciudad Valles, Carretera al Ingenio Plan de Ayala Km. 2, Colonia Vista Hermosa, C.P. 79010, Ciudad Valles, S.L.P.

ID 1st Author: *Dulce Carolina, Acosta-Pintor* / **ORC ID**: 0000-0003-0784-7039**, Researcher ID Thomson**: T-3349-2018, **arXiv Author ID**: DulceAcosta, **CVU CONACYT ID**: 626925

ID 1st Co-author: *Cuitláhuac, Mojica-Mesinas* / **ORC ID**: 0000-0001-8585-8249, **Researcher ID Thomson**: T-3267-2018, **arXiv Author ID**: MOMC640319JF8, **CVU CONACYT ID**: 744041

ID 2nd Co-author: *Eleazar, Vidal-Becerra* / **ORC ID**: 0000-0003-3857-2103, **Researcher ID Thomson**: T-1547-2018, arXiv Author ID: elia.vidal, **CVU CONACYT ID**: 623037

ID 3rd Co-author: *Jonathan de Jesús Constantino, González-Zarazúa* / **ORC ID**: 0000-0002-8386-225X, **arXiv Author ID**: Jonathan19, **CVU CONACYT ID**: 1167523

DOI: 10.35429/JOES.2021.25.8.22.29 Received 09 July, 2021; Accepted 28 November, 2021

Abstract

This paper documented the design, construction and operation test of a floating hood biodigester prototype, using organic residues (ruminal content, blood, bovine excreta and viscera) from the municipal trail of Ciudad Valles, S.L.P., with the purpose of generating biogas. The components of the biodigester system considered were: loading duct, concrete biodigester tank, biogas pipeline, floating hood, gas reservoir, discharge duct and discharge tank. A biodigester with storage capacity in the 0.178 m^3 floating hood was designed for a 30-day trial operation and storage of 0.120 m^3 of organic waste mixture in the biodigester tank. As of day 17 of operation the daily average of biogas generated was 0.1801 m^3. The composition of the biogas at day 30 of operation, showed a content of 59.4% of CH_4. When performing the flame test, an intense blue coloration was obtained, which indicates that the biogas produced has a high calorific value that will allow heating and flammability.

Biodigester, Floating hood, Organic waste, Municipal trail

Resumen

En este trabajo se documentó el diseño, construcción y prueba de funcionamiento de prototipo biodigestor de campana flotante, utilizando residuos orgánicos (contenido ruminal, sangre, excretas de ganado bovino y trozos de vísceras) del rastro municipal de Ciudad Valles, S.L.P., con la finalidad de generar biogás. Los componentes del sistema biodigestor considerados fueron: conducto de carga, tanque biodigestor de concreto, tubería de conducción de biogás, campana flotante, reservorio para gas, conducto de descarga y tanque de descarga. Se diseñó un biodigestor con capacidad de almacenamiento en la campana flotante de 0.178 m^3 para una operación de 30 días de prueba y almacenamiento de 0.120 m^3 de mezcla de residuos orgánicos en tanque biodigestor. A partir del día 17 de operación el promedio diario de biogás generado fue de 0.1801 m^3. La composición del biogás al día 30 de operación, mostró un contenido de 59.4% de CH_4. Al realizar la prueba de llama, se obtuvo una coloración azul intensa, lo que indica que el biogás producido posee un alto poder calorífico que permitirá el calentamiento e inflamabilidad.

.

Biodigestor, Campana flotante, Residuos orgánicos

Citation: ACOSTA-PINTOR, Dulce Carolina, MOJICA-MESINAS, Cuitláhuac, VIDAL-BECERRA, Eleazar and GONZÁLEZ-ZARAZÚA, Jonathan de Jesús Constantino. Design, construction and testing of a floating hood biodigester prototype for municipal waste organic waste. Journal of Experimental Systems. 2021. 8-25: 22-29

* Correspondence to Author (email: dulce.acosta@tecvalles.mx)
†Researcher contributing as first Author.

1. Introduction

In meat production, slaughterhouses are an important link in the production chain. In Mexico, there are 864 slaughterhouses and/or slaughter centers and 464 TIF slaughterhouses. Of these, in the State of San Luis Potosí there are 23 municipal slaughterhouses, two private slaughterhouses and eight TIF slaughterhouses (SENASICA, 2020).

The municipal slaughterhouse in Ciudad Valles, S.L.P. currently provides public slaughter services for cattle and swine. During slaughter, significant amounts of liquid and solid waste are generated, such as blood, urine, milk, gastrointestinal contents, bile, pieces of tissue, fat, hair, hooves, horns, etc., which are dragged with the water used for washing during and after slaughter to the collection and separation systems for solids, resulting in the presence of a variety of contaminants: physical, chemical, biological and microbiological.

According to a waste quantification study previously conducted at the municipal slaughterhouse, it was estimated that 21,388 kg of organic waste were generated per month, which represents 1,336.7 kg per day (16 days of waste generation), mainly a mixture of manure, bovine and pig blood, and bovine rumen content, so it is feasible to produce up to 1,625.95 m3 of biogas per month (Vidal, 2021).

It was identified that liquid waste (water and blood) is sent to the municipal wastewater treatment plant and solid waste from rumen, manure, hoof, tail and horns are taken to the sanitary landfill; this situation represents, in addition to the obvious environmental damage, a great waste of resources that can be valorized for biogas generation or can be considered a byproduct of slaughter. Due to the physical and chemical characteristics of the organic wastes derived from the slaughterhouse, they can be used and exploited for the generation of biogas.

The purpose of this work was to design and build a prototype floating hood biodigester to test the operation of organic waste digestion and evaluate its performance.

The reason why the study of the operation of this type of biodigester is required is because of the advantages it represents for the specific case of the municipal slaughterhouse of Ciudad Valles, considering that it has a limited space in the extension of land for the implementation of a taiwan or lagoon type biodigester. The floating bell biodigester has several advantages such as: years of useful life, smaller space requirement, vertical location, ease of maintenance and more durable construction materials (Hernández, A. 2013), which could be considered when implementing a project of this type in the field.

Methodology to be developed

For the design, construction and testing of the floating bell biodigester prototype, it was necessary to carry out four methodological stages:

Stage 1. Design of the prototype floating hood biodigester

For the realization of the prototype design, the ideation of the system was considered, and the following components were determined to degrade the biomass in single phase:

1. Loading duct: allows the biomass to enter from the load to the digester.
2. Concrete biodigester tank: where the decomposition of the biomass will be carried out according to the established retention time in the total absence of oxygen.
3. Biogas conduction piping: to transport the biogas from the digester to the floating bell.
4. Floating hood: made of galvanized sheet to allow the handling of biogas recovery.
5. Gas reservoir: bag for storage of the biogas generated.
6. Discharge duct: allows the exit of the stabilized material (sludge) after having completed the retention time inside the digester.
7. Discharge tank: this tank allows the accumulation of effluent and sludge as by-products of biomass biodegradation for later use.

ISSN 2410-3950

ACOSTA-PINTOR, Dulce Carolina, MOJICA-MESINAS, Cuitláhuac, VIDAL-BECERRA, Eleazar and GONZÁLEZ-ZARAZÚA, Jonathan de Jesús Constantino. Design, construction and testing of a floating hood biodigester prototype for municipal waste organic waste. Journal of Experimental Systems. 2021

Once the system components were identified, the dimensions of the prototype were determined based on the mixing ratio to be used in the biodigester for a 30-day test operation. For this purpose, the calculations suggested by García, J. and León E. 2015 were used.

The design of the floating bell biodigester prototype considered its operation with a daily load in a 1:3 ratio of 1 kg of organic waste obtained from the municipal slaughterhouse of Ciudad Valles and 3 l of water. The volume of the biodigester tank was sized to allow the digestion of 4 kg of mixture per day in 30 days of operation according to the following equation:

$$Vtb = CD * TR \quad (1)$$

Where:
Vtb =Volume of the biodigester tank (m^3).
CD =Daily load (kg)
TR = Time in which the mixture remains inside the biodigester (days)

$$\boldsymbol{Vtb = \left(\frac{4kg}{day} * \frac{1m^3 mix}{1000\ l\ mix}\right) 30\ days = 0.12 m^3}$$

The mixture to be deposited in the loading tank will have a volume of 0.120 m3 in 30 days of operation. But it must be considered that this mixture will occupy 75% and the remaining 25% will be occupied by the biogas generated. Therefore, a calculation was made to determine the total volume required with equation 2:

$$Vnb = Vtb + Vtb * \left(\frac{25}{100}\right) \quad (2)$$

Where:
Vnb = net volume of the biodigester tank (m^3).
Vtb = biodigester tank volume (m^3)
25% = remaining percentage to be taken up by the biogas generated

$$Vnb = 0.120m^3 + 0.120m^3 * \left(\frac{25}{100}\right) = 0.150\ m^3$$

The net volume of the biodigester tank necessary to deposit the raw material for 30 days was calculated at 0.150 m^3. In the case of this prototype, a concrete pipe was used as a biodigester tank. The calculated volume of the concrete pipe purchased and used for the biodigester meets the volume required to conserve the organic mixture.

For the sizing of the floating hood, the measurements of the biodigester tank were considered, calculating the diameter of the hood with the following equation:

$$\emptyset\ hood = \emptyset\ biodigester\ tan - 0.02\ m \quad (3)$$

Where:
$\emptyset\ hood$= hood diameter (m)
$\emptyset\ biodigester\ tank$ = biodigester tank diameter (m)
0.02 = decrease to biodigester tank diameter (m)

$$\emptyset\ hood = 0.44m - 0.02\ m = 0.42\ m$$

The diameter of the bell was calculated to be 0.42 m. In addition, the height of the floating hood was determined to be 0.30 m, less than the total height of the biodigester tank, that is, 1.15 m in height from its base to the beginning of the dome and 0.21 m the height of the floating hood dome, to obtain by equation 4, the total height of the floating hood from the following equation:

$$HT_{hood} = H_{hood} + H_{dome} \quad (4)$$

Where:
HT_{hood}= floating hood height (m)
H_{dome} = floating hood dome height (m)

$$HT_{hood} = 1.15 + 0.21 = 1.36\ m$$

With these data, the radius of curvature of the dome was obtained by the following equation:

$$R_{curv} = \frac{(r_{hood})^2 + (h_{dome})^2}{2(h_{dome})} \quad (5)$$

Where:
r_{hood}= hood radius (m)
h_{dome}= dome height (m)

$$R_{curv} = \frac{(0.21)^2 + (0.21)^2}{2(0.21)} = 0.21\ m$$

The radius of curvature of the dome was calculated to be 0.21 m. To obtain the volume of the bell and the volume of the bell dome, equations 6 and 7 were applied:

$$V_{hood} = \pi h r^2 \quad (6)$$

Where:
h= height of the hood (m)
r= hood radius a (m)

ISSN 2410-3950

$$V_{hood} = \pi(1.15)(0.21)^2 = 0.159\ m^3$$

$$V_{dome} = \pi(h_{cup})^2(R_{curv} - \frac{h_{cup}}{a}) \quad (7)$$

Where:
h_{dome} *= height of the dome (m).*
R_{curv} *= radius of curvature (m)*
a *= 3 constant value*

$$V_{dome} = \pi(0.21)^2(0.21 - \frac{0.21}{3}) = 0.0193\ m^3$$

The volume of the bell and the dome were calculated as 0.159 m^3 and 0.0193 m^3 respectively. With these data obtained, the total volume of the floating bell according to the following equation was considered to be:

$$Vt_{hood} = V_{hood} + V_{dome} \quad (8)$$

$$Vt_{hood} = 0.159 + 0.0193 = 0.178\ m^3$$

The design of the hood considers a total storage volume of 0.178 m^3, which will be sufficient to cover the calculated theoretical daily capacity of 0.0760 m^3 of biogas generated from municipal slaughterhouse waste. With this data, the design and dimensions of the biodigester prototype were elaborated in AutoCAD.

Stage 2 Construction of the floating bell biodigester prototype

The construction of this biodigester prototype was carried out within the Ciudad Valles Campus, where space, water and security were provided for access to it. The nursery area of the Campus was chosen with an extension of 330 m², the site was cleaned by removing the weeds, the area of approximately 58.9 m² was delimited for the construction of the prototype and the land was excavated with the support of hand tools, considering a vertical area of 1m for the subsequent placement of the biodigester.

For the construction of the biodigester tank, a 1.45 m long concrete pipe with a diameter of 0.44 m and a thickness of 3 inches was prepared; two 0.08 m diameter holes were drilled to allow the biomass to enter the biodigester and the effluents to exit.

Subsequently, the bottom of the excavation was tiled using wire mesh, cement, gravel and sand to lay the base of the concrete pipe, waiting for it to set for 24 hours, after which the sealing was verified. The concrete structure was waterproofed internally and externally to prevent future leaks during the operation (see Figure 1).

Figure 1 Tiling and placement of the concrete pipe
Own Source

The biodigester tank was also fitted with 3-inch PVC pipes sealed with silicone and white cement to supply and discharge the effluents. A straight slope was considered in the ducts to prevent the materials from clogging and thus facilitate maintenance during operation (see Figure 2). A 20-liter container connected to the duct was used as a discharge tank.

Figure 2 Placement of loading and unloading ducts
Own Source

For the construction of the biodigester's floating hood, 28-gauge galvanized steel sheet with a conical finish was used, with a total height of the hood of 1.36 m (1.15 m hood height and 0.21 m dome height), and a diameter of 0.42 m. The separation between the walls of the biodigester and the dome was 0.42 m.

ISSN 2410-3950

The separation between the walls of the biodigester and the body of the floating hood was aligned at 0.02 m, in order to allow it to rise and fall normally once the biodigestion process generates biogas. The floating hood was also waterproofed internally and externally to avoid possible leaks. Once finished, it was inserted into the biodigester (see Figure 3).

Figure 3 Placement of the floating hood
Own Source

The biogas conduction pipe was installed from the floating hood, using a ½" PVC pipe, 0.40 m long, which was connected to a ½" valve to control the gas outlet directly from the hood. The connection to the reservoir was made with a ½" by 0.40 m long hose for the conduction of biogas from the floating bell to the reservoir. A geomembrane was considered for the reservoir with a storage capacity of 0.178 m3. For the water column meter, a ½" by 0.10 m long PVC pipe, a ½" coupling and a ½" by 0.02 m long PVC pipe were connected to measure the pressure of the biodigester system.

Finally, a hydrostatic test was performed to verify possible leaks in the biodigester, where the biodigester was filled with water and all of its elements were checked. Each connection was reinforced with insulating tape to avoid possible leaks that could alter the gas transport. (See figure 4).

Figure 4 Floating hood biodigester prototype
Own Source

Stage 3 Monitoring of operating conditions during waste degradation

Organic waste from the municipal slaughterhouse was fed for 30 consecutive days starting on June 8, 2021. To feed the biodigester, a 1:3 mixture was made, 1 kg of organic waste obtained from the municipal slaughterhouse (rumen content, blood, cattle excrement and pieces of viscera), and 3 l of water, which was homogenized to enter through the biodigester loading duct (see Figure 5). A daily record was made of the amount of mixture loaded into the biodigester, pH and daily temperature to monitor the conditions of biogas production, the measurements were made with OAKTON PCD650 multiparametric equipment.

Figure 5 Preparation of organic waste and loading to biodigester
Own Source

ISSN 2410-3950

ACOSTA-PINTOR, Dulce Carolina, MOJICA-MESINAS, Cuitláhuac, VIDAL-BECERRA, Eleazar and GONZÁLEZ-ZARAZÚA, Jonathan de Jesús Constantino. Design, construction and testing of a floating hood biodigester prototype for municipal waste organic waste. Journal of Experimental Systems. 2021

The water column (mmWC) was also measured to calculate the biogas production generated from day 14 of operation. A Multitec model 540 device was used to measure biogas quality on day 30 of biodigester operation (see Figure 6).

Figure 6 Biogas quality monitoring
Own Source

The following physical-chemical parameters of the rumen content mixture to be used in biodigestion were also analyzed: pH, % moisture, % total solids, % ash, % volatile solids, % lipids, % carbon, % nitrogen, carbon/nitrogen ratio.

Stage 4. Flame test

After 15 days of the initial load, it is recommended to start verifying the beginning of biogas production (CO2 and CH4 in similar proportion), by means of the "biogas burning" verification. (FAO, 2011), so a flame test was performed.

3. Results

The results of each of the stages of the research were as follows:

Stage 1 and 2. Design and construction of prototype floating bell biodigester

A biodigester was designed with a storage capacity in the floating hood of 0.178 m3 for a 30-day test operation and storage of 0.120 m3 of organic waste mixture in the biodigester tank; considering that 1.0 kg of waste theoretically generates 0.0760 m3 of biogas per day.

Stage 3 Monitoring of operating conditions during waste degradation

A record of the amount of mixture poured into the biodigester, pH and daily temperature was made to monitor the biogas production conditions. Table 1 shows the results of the records observed. It should be noted that in this prototype biogas production began on day 14 of feeding, during which time the pressure was measured in mmCA and the volume of biogas generated in liters for 17 days, exceeding expectations of biogas production with an average of 0.1801 m3, so that the biodigester was depressurized on a daily basis. The results are shown in Table 2.

Day	kg feed: 1kg beef/3 l water	pH	Temperature °C
08/06/2021	4	7.11	24.6
09/06/2021	4	7.08	27.7
10/06/2021	4	7.09	25.7
11/06/2021	4	7.08	25.6
12/06/2021	4	7.09	24.8
13/06/2021	4	7.1	29.4
14/06/2021	4	7.1	26.2
15/06/2021	4	7.11	24.7
16/06/2021	4	7.1	27.3
17/06/2021	4	7.08	26.6
18/06/2021	4	7.12	27.2
19/06/2021	4	7.13	28
20/06/2021	4	7.14	25.8
21/06/2021	4	7.15	31.6
22/06/2021	4	7.15	25.5
23/06/2021	4	7.14	23.6
24/06/2021	4	7.14	23.4
25/06/2021	4	7.12	25.1
26/06/2021	4	7.04	24.5
27/06/2021	4	7.08	24.6
28/06/2021	4	7.13	21.1
29/06/2021	4	7.13	27.5
30/06/2021	4	7.15	24.6
01/07/2021	4	7.13	24.5
02/07/2021	4	7.13	25.2
03/07/2021	4	7.12	26.2
04/07/2021	4	7.13	23.8
05/07/2021	4	7.12	23.2
06/07/2021	4	7.12	22.4
07/07/2021	4	7.11	24.8
Average	4	7.114	25.50

Table 1 Quantities of organic matter introduced into the biodigester
Own Source

ISSN 2410-3950

Day	mmCA	m^3 biogas produced
21/06/2021	52	0.1794
22/06/2021	34	0.1790
23/06/2021	138	0.1810
24/06/2021	66	0.1796
25/06/2021	150	0.1812
26/06/2021	126	0.1807
27/06/2021	136	0.1809
28/06/2021	140	0.1810
29/06/2021	128	0.1808
30/06/2021	116	0.1805
01/07/2021	108	0.1804
02/07/2021	98	0.1802
03/07/2021	86	0.1800
04/07/2021	72	0.1797
05/07/2021	60	0.1795
06/07/2021	44	0.1792
07/07/2021	20	0.1787
Average	92.5883	0.1801

Table 2 Monitoring of mmCA and calculation of m^3 biogas produced
Own source

On the 30th day of operation, a biogas quality measurement was carried out with a Multitec model 540 meter, where the biogas composition was identified. The results are shown in Table 3.

Biogas composition	Results	Biogas composition	Results
Methane (CH_4)	59.4%	Methane (CH_4)	59.4%
Carbon dioxide (CO_2)	37%	Carbon dioxide (CO_2)	37%
Hydrogen sulfide (H_2S)	0.20 %	Hydrogen sulfide (H_2S)	0.20 %

Table 3 Composition of biogas measured with Multitec model 540

According to Varnero and Arellano (1991), for the process to develop satisfactorily, the pH value in the digester not only determines the biogas production but also its composition (pH should not fall below 6.0 or rise above 8.0). A pH value below 6 indicates that the biogas generated is very poor in methane and therefore has lower energetic qualities. When the biogas has a methane content higher than 45%, it is flammable (FAO, 2011). Table 1 shows pH conditions that allow methane generation, and Table 3 shows the composition of the biogas at day 30 of operation, showing 59.4% CH_4, which indicates flammability. The results of the physical-chemical parameters performed to the rumen content mixture of municipal slaughterhouse, are very close to the references of Falla, 1995 and Gonzalez, 2018.

The rumen content of the municipal slaughterhouse presented a pH of 7.11 close to neutrality, which is a determining factor in the methanogenic process. The calculated moisture percentage was 88.15%, the percentage of solid matter (ST) was 11.85% and volatile solids (SV) were quantified at 87.2%. The ratio of carbon and nitrogen content is 22/1, which increases the production of bacteria to generate optimal conditions for biogas production.

Parameter	Rumen content mix	Reference	
pH	7.11	6.5-7.5	Falla, L.
% Humidity	88.15	85	Falla, L.
% ST	11.85	14.63	González, R.
% Ash	12.8	27.06	Falla, L.
% SV	87.2	81.16	González, R.
% Lipids	4.54	9.60	Falla, L.
% C	22	20	Falla, L.
% N	1	1	Falla, L.
C/N	22/1	20/1	Falla, L.

Table 4 Physicochemical parameters of rumen content at the municipal slaughterhouse
Own Source

Stage 4. Flame test

A small burner was attached to the biogas outlet hose, testing its ignition. Figure 7 shows the intense blue coloration obtained from the flame on the 30th day of operation of the biodigester, which indicates that the biogas has a high calorific value, which will allow heating and flammability. If the gas burns with a bluish flame and good consistency, normal use of the biogas can be initiated (FAO, 2011).

Figure 7 Flame test, intense blue coloration
Own Source

ISSN 2410-3950

4. Acknowledgements

We would like to thank the Rastro Municipal de Ciudad Valles that collaborated with the contribution of the residues for this research, as well as the Chemistry Laboratory of the Instituto Tecnológico de Ciudad Valles, for the facilities provided for the physical-chemical analysis of the rumen content.

5. Conclusions

The floating bell biodigester prototype demonstrated that the organic waste (rumen content, blood, cattle excreta and viscera pieces) from the municipal slaughterhouse generates an important percentage of methane (CH_4) in the anaerobic digestion process, and can be captured in a reservoir to be used later in the water heating processes for carcass dressing and cleaning of the facilities. In addition, the characteristics of this biodigester system are adapted to the situation of lack of space in the municipal slaughterhouse.

The average daily biogas production of $0.180m^3$ obtained in this prototype demonstrates that it is possible to obtain a higher percentage of biogas production with organic waste. Once these results are obtained, a feasibility study is expected to be carried out for a floating bell biodigester system according to the amount of organic waste generated monthly at the municipal slaughterhouse that considers the implementation costs of a project of this magnitude.

6. References

Dirección General de Inocuidad Agroalimentaria, Acuícola y Pesquera. 2020. *Directorio de Establecimientos TIF*. Recuperado el 09 de mayo del 2021 https://dj.senasica.gob.mx/SIAS/Statistics/Inocuidad/EstabTIF

Dirección General de Inspección Fitozoosanitaria. 2020. *Listado de Rastro y/o Centros de matanza en los que se realiza vigilancia o seguimiento operativo por parte de las entidades federativas.* Año 2020. Recuperado el 09 de mayo del 2021 https://www.gob.mx/senasica/documentos/directorio-de-padron-de-rastros

Falla, L. (1995). *Desechos de matadero con alimento animal en Colombia*. Frigorífico Guadalupe S. A. Santa fe de Bogotá Colombia.

García, J. y León E. (2015). *Diseño y construcción de un biodigestor hindú Anaerobio en la finca Los Cuencanos de la Parroquia García Moreno.* [Tesis de Licenciatura]. Escuela Superior Politécnica de Chimborazo, Ecuador. Repositorio Institucional DSpace ESPOCH http://dspace.espoch.edu.ec/handle/123456789/4863.

González, R. (2018). *Estudio de Factibilidad para la Producción de Biogás a Partir de los Residuos Orgánicos del Rastro Municipal de Juigalpa, Nicaragua*. (ONUDI)

Hernández, A. (2013). *El potencial de los biodigestores como técnica sostenible para la producción de biogás en la Comunidad Indígena Nuevo San Juan Parangaricutiro, Michoacán.* [Tesis de Licenciatura]. Universidad Autónoma del Estado de México Facultad de Planeación Urbana y Regional. Repositorio Institucional RI. http://hdl.handle.net/20.500.11799/58557.

Varnero, M.T. FAO (2011). *Manual del Biogás*. Santiago, Chile. ISBN 978-95-306892-0 .Proyecto FAO.

Varnero, M.T. y Arellano, J. 1990. *Aprovechamiento racional de desechos orgánicos. Ministerio de Agricultura (FIA).* Universidad de Chile. Facultad de Ciencias Agrarias y Forestales, Informe Técnico. Santiago, Chile, 98p.

Vidal, E.,Mojica, C.,Acosta, D.C., Reyes, A.(2021). *Estudio de los residuos orgánicos de un rastro municipal, para su aprovechamiento en la generación de energía calorífica*. Congreso Internacional de Investigación de Academia Journals Puebla 2021 Vol. 13, No. 7.

Article **Journal of Experimental Systems**
December, 2021 Vol.8 No.25 30-36

Percepción remota y procesamiento de imágenes para la gestión de cultivos de caña de azúcar

Remote perception and image processing for the management of sugar cane crops

LÁRRAGA-ALTAMIRANO, Hugo Rene†*, HERNÁNDEZ-LÓPEZ, Dalia Rosario, PIEDAD-RUBIO, Ana María and AMADOR-SONI, Jesús Antonio

Tecnológico Nacional de México, Campus Ciudad Valles

ID 1st Author: *Hugo Rene, Lárraga-Altamirano* / **ORC ID**: 0000-0001-8258-9418, **Researcher ID Thomson**: T-2296-2018, **arXiv Author ID**: Hugo_Larraga, **CVU CONACYT ID**: 626539

ID 1st Co-author: *Dalia Rosario, Hernández-López* / **ORC ID**: 0000-0002-2751-5886, **Researcher ID Thomson**: T-2470-2018, **arXiv Author ID**: DaliaHernandez, **CVU CONACYT ID**: 536472

ID 2nd Co-author: *Ana María, Piedad-Rubio* / **ORC ID**: 0000-0003-1258-0383, **Researcher ID Thomson**: T-2477-2018, **arXiv Author ID**: ampiedad, **CVU CONACYT ID**: 732279

ID 3rd Co-author: *Jesús Antonio, Amador-Soni* / **ORC ID**: 0000-0002-7264-6148, **arXiv Author ID**: sonibaba, **Open ID**: 106324682174175915693, **CVU CONACYT ID**: 1167881

DOI: 10.35429/JOES.2021.25.8.30.36 Received 09 July, 2021; Accepted 28 December, 2021

Abstract

This research work shows that with the use of remote sensing technology it is possible to more effectively fulfill two of the purposes pursued by farmers in the field; manage crops more efficiently and include environmental care in decision-making. Specifically, remote sensing is applied in the context of precision agriculture through geographic information systems (GIS), unmanned aerial vehicles (UAV), multispectral sensors that capture the reflectance of the infrared band of the light spectrum (for interpretation of the biochemical state of the crop), global geopositioning systems (GPS), among others. This study limits the use of this technology to the processing of multispectral images obtained by aerial photogrammetry, and its subsequent treatment for the generation of orthoimages, the calculation of the NDVI vegetation index and the classification of land cover by clustering. Finally, the effect of classification with RGB and multispectral images is analyzed.

Remote sensing, Clustering, GIS, UAV, NDVI

Resumen

El presente trabajo de investigación demuestra que con la utilización de tecnología de percepción remota es posible cumplir con mayor eficacia dos de los propósitos que persiguen los productores del campo: administrar los cultivos con mayor eficiencia e incluir el cuidado ambiental en la toma de decisiones. Específicamente, la percepción remota es aplicada en el contexto de la agricultura de precisión mediante sistemas de información geográfica (SIG), vehículos aéreos no tripulados (VANT), sensores multiespectrales que captan la reflectancia de la banda infrarroja del espectro de luz (para la interpretación del estado bioquímico del cultivo), sistemas de geoposicionamiento global (GPS), entre otros. Este estudio acota el uso de esta tecnología al procesamiento de imágenes multiespectrales obtenidas por fotogrametría aérea, y su tratamiento posterior para la generación de ortoimágenes, el cálculo del índice de vegetación NDVI y la clasificación de coberturas terrestres por clusterizacion. Por último, se analiza el efecto de la clasificación con las imágenes RGB y multiespectral.

Percepción remota, Clusterizacion, SIG, VANT, NDVI

Citation: LÁRRAGA-ALTAMIRANO, Hugo Rene, HERNÁNDEZ-LÓPEZ, Dalia Rosario, PIEDAD-RUBIO, Ana María and AMADOR-SONI, Jesús Antonio. Percepción remota y procesamiento de imágenes para la gestión de cultivos de caña de azúcar. Journal of Experimental Systems. 2021. 8-25: 30-36

* Correspondence to Author (e-mail: hugo.larraga@tecvalles.mx).
†Researcher contributing as first Author.

1. Introduction

Sugarcane is the crop with the highest production worldwide, in Mexico alone in 2017, 772,003 hectares were harvested which produced 56,954,993 tons of this grass mostly used by the sugar industry (FAO, 2019). In the Huasteca Potosina region located in the state of San Luis Potosí, agriculture is the main economic activity, with the cultivation of sugarcane standing out from others, such as corn, beans, sorghum, fruits and citrus (Aparicio, 2013).

Therefore, the efficient and sustainable production of sugarcane is an important issue, since on the one hand there is a tendency to better manage the field with fewer resources and, on the other, to reduce the negative impact of agricultural activities on planetary care. In other words, farmers must make decisions based on a greater amount of information to ensure economic viability without neglecting environmental friendliness. Information and communication technologies play a central role in the construction of intelligent farm models that provide the producer with information acquired from different media, allowing to monitor the plots in real time to plan their activities in response to changing circumstances (O'Grady, M. & O'Hare,M., 2017).

The present research work helps to achieve more effectively the two aforementioned purposes; to manage crops more efficiently and to include environmental care in decision making. Specifically, remote sensing is applied in the context of precision agriculture through geographic information systems (GIS), unmanned aerial vehicles (UAVs), multispectral sensors that capture the reflectance of the infrared band of the light spectrum (for the interpretation of the biochemical status of the crop), global geopositioning systems (GPS), among others (O'Grady, M. & O'Hare,M., 2017).

This technology for the acquisition and processing of sensed data gives support to crop management, in activities such as: pest detection, fertilizer use, productivity variation, yields, soil chemistry, to mention some of the factors that are of interest to producers (Aguilar, 2015).

Currently, different technological solutions are implemented to obtain information on crops and thus create an intelligent model for their management, each of which makes use of sophisticated measuring equipment, either to know the moisture level in the soil, the temperature or the nutritional status of the plant through sensor networks, satellites, airships, among others (Aparicio, 2013). However, this study The objective of this work is to apply remote sensing and image processing techniques for monitoring sugarcane crops.

This includes, the operation of UAVs, the integration of crop orthoimages ("map"), with multispectral information to calculate the normalized difference vegetation index (NDVI) and land cover classification by clustering. The above tasks generate a mass of data useful for field producers (Majumdar, Naraseeyappa, & Ankalaki, 2017). The latter allows analyzing the effect of classification with RGB and multispectral images. Each stage of development integrates technology that requires estimations to be made to adapt to sugarcane monitoring in the Huasteca Potosina region, so that producers will have a greater amount of data that favors efficient decision making (Cheli, 2011).

2. Methodology

Agriculture depends on many climatic, geographical, biological, political and economic factors, which introduce risks. Processed crop information is part of the efficient management of these risks, which is essential for successful agricultural production. Effective information management allows estimating the probability of undesirable situations and minimizing the consequences. Therefore, reliable information on historical crop yields is vital for decisions related to agricultural risk management (A.A. & R.V., 2013).

For the development of the project, 3 stages were defined, as shown in Figure 1.

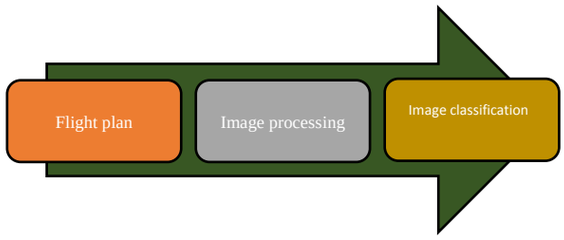

Figure 1 Methodology
Source: Own

ISSN 2410-3950

2.1 Flight Plan

It is important to observe the presence of obstacles, their heights and locations, wind conditions, infrastructure that generates electromagnetic radiation, as well as the extension (area and shape) so that the calculation of the photogrammetric parameters is accurate. It is possible to execute a reconnaissance flight with the assistance of a flight control software that helps to estimate the aforementioned information, locate the point of origin (HOME POINT), the appropriate altitude and the type of trajectory to follow, take-off and landing zone, estimated flight time, among others.

The geographic location of the area to be covered is obtained through a geospatial information system (GIS) such as Google Earth, which allows the construction of .KML or .KMZ files useful for the planning of autonomous flights. Another option is to determine the territorial coverage with the autonomous flight software, in this case Pix4D Capture will be used because of its easy operation and high efficiency. Both software can interact together to calculate the geographic coordinates that delimit the crop to be inspected, as well as to configure some of the parameters required for the flight such as: overlapping minimum, intermediate speed depending on the drone model, camera angle, orientation and flight altitude (González, Amarillo, Amarillo, & Sarmiento, 2015).

The calibration of the aircraft sensors, as well as the correct configuration of the RGB and multispectral cameras are key aspects to perform a flight under standardized safety conditions and obtain the appropriate quantity and quality of images for further processing (Herrero Huerta, 2016).

2.2 Image processing

The map construction process is performed with the widely recognized processing or transformation software Pix4D Mapper. The images obtained are used to generate cartographic products such as: reflectance map, elevation model, point cloud, among others. In turn, the multispectral images formed by the light reflection of the red, near infrared, infrared and green bands create the NDVI index map used in precision agriculture to determine crop conditions.

Geographic information systems process the images using the geospatial data attached in the metadata by combining them, much like integrating a mosaic, to present a single image (orthoimage) of the crop (Tapia Arenas, Guevara Bonilla, & Esquivel Segura, 2019). It is important to note that multispectral images are affected by some factors that change during each shot, such as clouds, time of capture, altitude and illumination, so in order to have greater accuracy a radiometric correction is required using control images taken designed for the type of camera.

2.3 Image classification

The classification of the mosaic created from the image processing has the purpose of distinguishing the vegetation units corresponding to the sugar cane crop, other types of vegetation and soil. The result of the previous phase is two ortho images of the crop, one in RGB bands and the other in NDVI bands. For the RGB classification, a supervised method called Minimum Distance is used, which uses mean spectral values of the different classes, ignoring the variances between them. (Willington, Nolasco, & Bocco, 2013). For this, the three training classes are first established: sugarcane (class 1), natural soil (class 2) and other vegetation (class 3), represented by buffers of pixels extracted from the original image.

On the other hand, the classification of the multispectral mosaic is performed with an unsupervised method known as k-means, which classifies a given set of objects into k-clusters (classes), each cluster is represented by the average of its points, i.e., its centroid (Cambronero, 2006). This method does not require training, in fact, the objective is to classify a set of pixels based on the similarity of their spectral characteristics.

2. Results

3.1 Flight plan

This phase comprises the performance of different activities, which are listed below:

1. Reconnaissance of the area to be flown. Before starting the flight, it is advisable that the pilots know the physical place where they will fly, this allows them to identify obstacles such as mountains, trees, towers, cables, among others.

ISSN 2410-3950

2. Firmware update. It is important that the vehicles have the latest firmware version and the database of safe flight zones updated. This process, as well as the safe flight databases, is achieved through the DJI Assistance 2 application, which offers an intuitive interface for DJI products. See Figure 2 and Figure 3.

Figure 2 DJI Assistence 2 firmware main window
Source: own

Figure 3 Firmware update status
Source: own

3. Geolocate the terrain to be studied. Using software support (Google Earth) it is recommended to locate the study area to obtain its geographic coordinates. The software has a useful search tool to identify the area to be explored, just type the name of the place or nearby places to get a view in Google Maps format. With the polygon tool, the study area can be delimited and a name can be added to identify it from other projects. See Figure 4 and Figure 5.

Figure 4 Geolocation of the firmware study area
Source: Google Earth

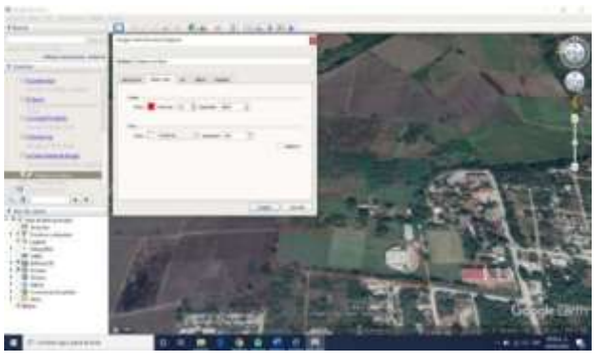

Figure 5 Delimitation of the firmware study area
Source: Google Earth

4. Calibration. To have an accurate flight it is necessary to perform the required calibrations to the equipment, this includes calibrating: compass, IMU, remote control and cameras. The calibration of the drone is done using the DJI Go application tools, it is recommended that the compass, IMU and remote control are in 'Normal' conditions before the flight. Additionally, the SEQUOIA multispectral camera should be configured and calibrated independently of the vehicle. See Figure 6 and Figure 7.

Figure 6 Sensor support
Source: Own

ISSN 2410-3950

Figure 7 Connection of the multispectral sensor
Source: Own

5. Programmed flight. The aerial route that the drone will take is programmed in the Pix4D Capture application from where the vehicle will be controlled.

3.2 Image processing

Image processing is a process that involves the use of specialized photogrammetry software. Highly complex algorithms join the photographs obtained by the UAVs to create cartographic products used in the study of crops such as: orthomosaics, maps, indexes, among others. In this case, the processing was performed by Pix4D Mapper, a market leader in photogrammetric applications. Figures 8 and 9.

Figure 8 Result of the RGB camera shot
Source: Pix4Dmapper

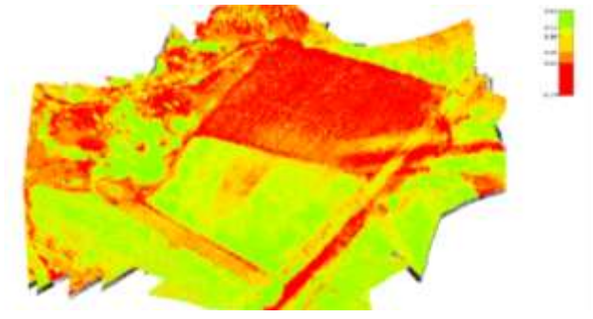

Figure 9 Multispectral camera acquisition result
Source: Pix4Dmapper: Pix4Dmapper

It is interesting to note that PIX4D offers 3 options to present the NDVI, which, in a way is also a classification of the calculated values. Equal Spacing classifies the NDVI using the same range of minimum and maximum values for all classes. Equal Area, distributes the land area among the number of classes showing the minima and maxima of each section. Jenks, an unsupervised classification algorithm that groups values with a similar Euclidean distance, uses the same principle as k-means, see Figure 10.

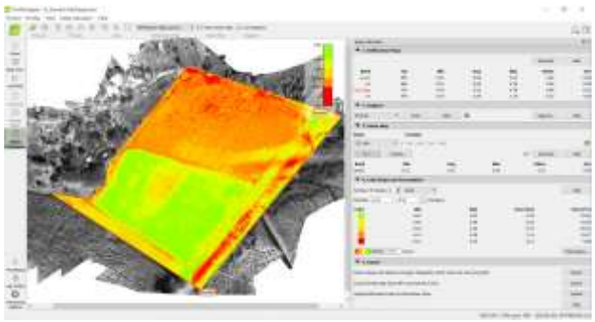

Figure 10 Jenks, clustering of values
Source: Pix4Dmapper

3.3 Image classification

The classification process involves the use of supervised and unsupervised algorithms operated from QGIS. For this particular case we want to identify the sugarcane crop as efficiently as possible considering that the orthoimages resulting from the previous step are RGB (three bands) and NDVI (single band), see Figure 8. For the training stage of the supervised technique three macro classes were created: sugarcane (green), soil (gray), other vegetation (yellow). The QGIS Semi-Automatic Classification Plugin (SCP) tool consists of a set of tools for classifying orthoimages. For each of these, four regions of interest were defined and then the Minimum Distance algorithm was run, the results are shown in Figure 11.

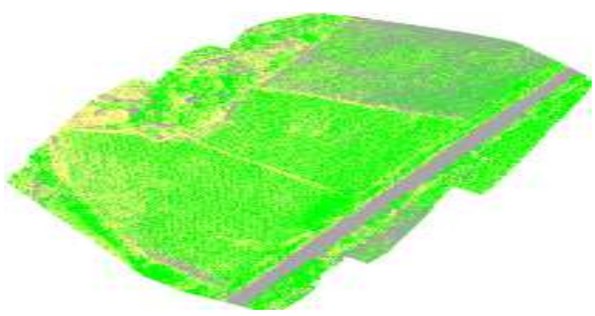

Figure 11 Classification by Minimum Distance RGB orthoimage
Source: QGIS

ISSN 2410-3950

The unsupervised classification was applied to the single band NDVI image. The Band Processing > Clustering tool of the SCP suite implements the k-means algorithm which groups pixels of the same reflectance level into as many groups as specified. For this example 5 groups were determined, the output shows the centroids of each group and the average distance between the pixels of each group, see Figure 12.

Clustering

Clase	Signature	Distance
C_ID_1	0.15215677267740985	0.002681066135040377 5
C_ID_2	0.24731779982238047	0.004296262696008773 5
C_ID_3	0.3777461161261149	0.004213452577450285
C_ID_4	0.5516033878977658	0.001770539684128325
C_ID_5	0.7091170809131433	0.000272041028348102 3

Figure 12 Example of centroid outputs
Source: QGIS

The image of the final result is interesting to analyze, it is observed that the vegetation is easily distinguished, both healthy and unhealthy, likewise it is shown that the arid soil and asphalt have similarities, see Figure 13.

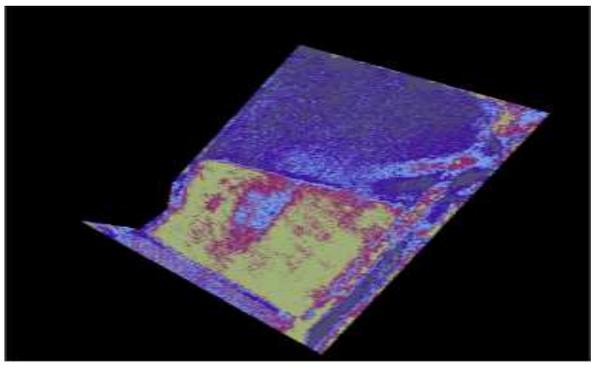

Figure 13 Classification using QGIS
Source: QGIS

3.4 Discussion of the results

The classification supervised by Minimum Distance on the RGB orthoimage, presents confusion between classes, i.e., in some groups of pixels it does not reliably distinguish whether they belong to the reed class or to another vegetation. Similarly, although with less error, the soil class is not identified when it borders with a large amount of other vegetation. It follows that the training process is costly in the sense that more samples per class are required to be labeled correctly.

The unsupervised k-means classification on the NDVI orthoimage clearly distinguishes the vegetation from the rest of the objects contained in the photograph. It is interesting to note that the spectral characteristics of the infrared band do indeed provide information that can be interpreted to assess crop condition. Even though there is confusion between the cane class and the other vegetation, the crop section shows more spectral details that can be analyzed to improve productivity.

4. Conclusions

This model presented involves the use of remote sensing and image processing techniques to obtain crop information. These remote sensing and image processing techniques can be applied to different types of crops. As a management model, the biochemical information of the agricultural crop expressed in NDVI values can be considered as a critical element to improve productivity, influencing decomposition processes and nutrient cycling, biochemical changes in the canopy, build a temporal database or be used with mathematical models for decision making in relation to input management and sugarcane management practices.

5. References

A.A., R., & R.V., K. (2013). Review- Role of Data Mining in Agriculture. *IJCSIT International Journal of Computer Science and Information Technologies*, 270-272.

Aguilar, N. (2015). Percepción remota como herramienta de competitividad de la agricultura. *Revista mexicana de ciencias agrícolas, 6*(2), 399-405.

Aparicio, F. &. (2013). Wireless Sensor Networks Applied to Optimization in Precision Agriculture for Coffee Crops in Colombia. *Journal de Ciencia e Ingeniería, 5*(1), 46–52.

Cambronero, C. G. (2006). Algoritmos de aprendizaje: knn & kmeans. *Intelgencia en Redes de Comunicación* (pág. 23). Madrid: Universidad Carlos III de Madrid.

Cheli, A. E. (2011). *Introducción a la Fotogrametría y su evolución.*

ISSN 2410-3950

FAO. (2019). *FAOSTAT*. Obtenido de FAOSTAT: http://www.fao.org/faostat/es/#home

González, A., Amarillo, G., Amarillo, M., & Sarmiento, F. (2015). Drones Aplicados a la Agricultura de Precisión. *Revista Especializada en Ingeniería*, 23-37.

Herrero Huerta, M. (2016). Fotogrametría de rango cercano aplicada a la Ingeniería Agroforestal. Salamanca, Guanajuato, México.

Majumdar, J., Naraseeyappa, S., & Ankalaki, S. (2017). Analysis of agriculture data using data mining techniques: application of big data. *Springer*, 1-15.

O'Grady, M., & O'Hare,M. (2017). Modelling the smart farm. *Information Processing in Agriculture, 4*(3), 179-187. doi://doi.org/10.1016/j.inpa.2017.05.001

Tapia Arenas, A., Guevara Bonilla, M., & Esquivel Segura, E. (2019). *Procesamiento de imágenes a partir de vehículos aéreos no tripulados utilizando software libre.* Costa Rica: Tecnológico de Costa Rica.

Willington, E., Nolasco, M., & Bocco, M. (2013). Clasificación supervisada de suelos de uso agrícola en la zona central de Córdoba (Argentina): comparación de distintos algoritmos sobre imágenes Landsat. *Congreso Argentino de AgroInformatica* (págs. 207-216). Argentina: JAIIO - CAI.

ISSN 2410-3950

[Title in Times New Roman and Bold No. 14 in English and Spanish]

Surname (IN UPPERCASE), Name 1st Author†*, Surname (IN UPPERCASE), Name 1st Coauthor, Surname (IN UPPERCASE), Name 2nd Coauthor and Surname (IN UPPERCASE), Name 3rd Coauthor

Institutional Affiliation of Author including Dependency (No.10 Times New Roman and Italic)

International Identification of Science - Technology and Innovation

ID 1st Author: (ORC ID - Researcher ID Thomson, arXiv Author ID - PubMed Author ID - Open ID) and CVU 1st author: (Scholar-PNPC or SNI-CONACYT) (No.10 Times New Roman)

ID 1st Coauthor: (ORC ID - Researcher ID Thomson, arXiv Author ID - PubMed Author ID - Open ID) and CVU 1st coauthor: (Scholar or SNI) (No.10 Times New Roman)

ID 2nd Coauthor: (ORC ID - Researcher ID Thomson, arXiv Author ID - PubMed Author ID - Open ID) and CVU 2nd coauthor: (Scholar or SNI) (No.10 Times New Roman)

ID 3rd Coauthor: (ORC ID - Researcher ID Thomson, arXiv Author ID - PubMed Author ID - Open ID) and CVU 3rd coauthor: (Scholar or SNI) (No.10 Times New Roman)

(Report Submission Date: Month, Day, and Year); Accepted (Insert date of Acceptance: Use Only ECORFAN)

Abstract (In English, 150-200 words)

Objectives
Methodology
Contribution

Abstract (In Spanish, 150-200 words)

Objectives
Methodology
Contribution

Keywords (In English)

Indicate 3 keywords in Times New Roman and Bold No. 10

Keywords (In Spanish)

Indicate 3 keywords in Times New Roman and Bold No. 10

Citation: Surname (IN UPPERCASE), Name 1st Author, Surname (IN UPPERCASE), Name 1st Coauthor, Surname (IN UPPERCASE), Name 2nd Coauthor and Surname (IN UPPERCASE), Name 3rd Coauthor. Paper Title. Journal of Experimental Systems. Year 1-1: 1-11 [Times New Roman No.10]

* Correspondence to Author (example@example.org)
† Researcher contributing as first author.

Introduction

Text in Times New Roman No.12, single space.

General explanation of the subject and explain why it is important.

What is your added value with respect to other techniques?

Clearly focus each of its features

Clearly explain the problem to be solved and the central hypothesis.

Explanation of sections Article.

Development of headings and subheadings of the article with subsequent numbers

[Title No.12 in Times New Roman, single spaced and bold]

Products in development No.12 Times New Roman, single spaced.

Including graphs, figures and tables-Editable

In the article content any graphic, table and figure should be editable formats that can change size, type and number of letter, for the purposes of edition, these must be high quality, not pixelated and should be noticeable even reducing image scale.

[Indicating the title at the bottom with No.10 and Times New Roman Bold]

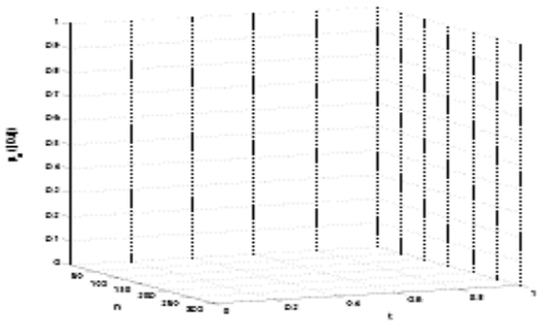

Graphic 1 Title and *Source (in italics)*

Should not be images-everything must be editable.

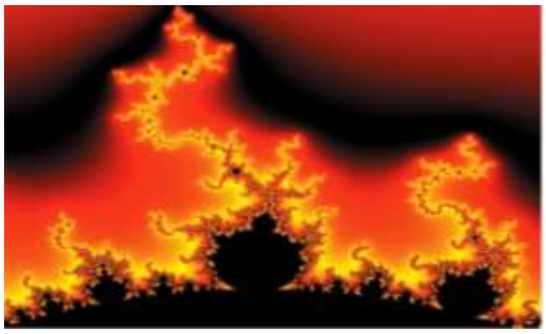

Figure 1 Title and *Source (in italics)*

Should not be images-everything must be editable.

Table 1 Title and *Source (in italics)*

Should not be images-everything must be editable.

Each article shall present separately in **3 folders**: a) Figures, b) Charts and c) Tables in .JPG format, indicating the number and sequential Bold Title.

For the use of equations, noted as follows:

$$Y_{ij} = \alpha + \sum_{h=1}^{r} \beta_h X_{hij} + u_j + e_{ij} \quad (1)$$

Must be editable and number aligned on the right side.

Methodology

Develop give the meaning of the variables in linear writing and important is the comparison of the used criteria.

Results

The results shall be by section of the article.

Annexes

Tables and adequate sources

Thanks

Indicate if they were financed by any institution, University or company.

Conclusions

Explain clearly the results and possibilities of improvement.

ISSN 2410-3950

References

Use APA system. Should not be numbered, nor with bullets, however if necessary numbering will be because reference or mention is made somewhere in the Article.

Use Roman Alphabet, all references you have used must be in the Roman Alphabet, even if you have quoted an Article, book in any of the official languages of the United Nations (English, French, German, Chinese, Russian, Portuguese, Italian, Spanish, Arabic), you must write the reference in Roman script and not in any of the official languages.

Technical Specifications

Each article must submit your dates into a Word document (.docx):

Journal Name
Article title
Abstract
Keywords
Article sections, for example:

1. Introduction
2. Description of the method
3. Analysis from the regression demand curve
4. Results
5. Thanks
6. Conclusions
7. References

Author Name (s)
Email Correspondence to Author
References

Intellectual Property Requirements for editing:

-Authentic Signature in Color of Originality Format Author and Coauthors

-Authentic Signature in Color of the Acceptance Format of Author and Coauthors

ISSN 2410-3950

Reservation to Editorial Policy

Journal of Experimental Systems reserves the right to make editorial changes required to adapt the Articles to the Editorial Policy of the Research Journal. Once the Article is accepted in its final version, the Research Journal will send the author the proofs for review. ECORFAN® will only accept the correction of errata and errors or omissions arising from the editing process of the Research Journal, reserving in full the copyrights and content dissemination. No deletions, substitutions or additions that alter the formation of the Article will be accepted.

Code of Ethics - Good Practices and Declaration of Solution to Editorial Conflicts

Declaration of Originality and unpublished character of the Article, of Authors, on the obtaining of data and interpretation of results, Acknowledgments, Conflict of interests, Assignment of rights and Distribution

The ECORFAN-Mexico, S.C Management claims to Authors of Articles that its content must be original, unpublished and of Scientific, Technological and Innovation content to be submitted for evaluation.

The Authors signing the Article must be the same that have contributed to its conception, realization and development, as well as obtaining the data, interpreting the results, drafting and reviewing it. The Corresponding Author of the proposed Article will request the form that follows.

Article title:

– The sending of an Article to Journal of Experimental Systems emanates the commitment of the author not to submit it simultaneously to the consideration of other series publications for it must complement the Format of Originality for its Article, unless it is rejected by the Arbitration Committee, it may be withdrawn.

– None of the data presented in this article has been plagiarized or invented. The original data are clearly distinguished from those already published. And it is known of the test in PLAGSCAN if a level of plagiarism is detected Positive will not proceed to arbitrate.

– References are cited on which the information contained in the Article is based, as well as theories and data from other previously published Articles.

– The authors sign the Format of Authorization for their Article to be disseminated by means that ECORFAN-Mexico, S.C. In its Holding Bolivia considers pertinent for disclosure and diffusion of its Article its Rights of Work.

– Consent has been obtained from those who have contributed unpublished data obtained through verbal or written communication, and such communication and Authorship are adequately identified.

– The Author and Co-Authors who sign this work have participated in its planning, design and execution, as well as in the interpretation of the results. They also critically reviewed the paper, approved its final version and agreed with its publication.

– No signature responsible for the work has been omitted and the criteria of Scientific Authorization are satisfied.

– The results of this Article have been interpreted objectively. Any results contrary to the point of view of those who sign are exposed and discussed in the Article.

Copyright and Access

The publication of this Article supposes the transfer of the copyright to ECORFAN-Mexico, SC in its Holding Bolivia for it Journal of Experimental Systems, which reserves the right to distribute on the Web the published version of the Article and the making available of the Article in This format supposes for its Authors the fulfilment of what is established in the Law of Science and Technology of the United Mexican States, regarding the obligation to allow access to the results of Scientific Research.

Article Title:

Name and Surnames of the Contact Author and the Coauthors	Signature
1.	
2.	
3.	
4.	

Principles of Ethics and Declaration of Solution to Editorial Conflicts

Editor Responsibilities

The Publisher undertakes to guarantee the confidentiality of the evaluation process, it may not disclose to the Arbitrators the identity of the Authors, nor may it reveal the identity of the Arbitrators at any time.

The Editor assumes the responsibility to properly inform the Author of the stage of the editorial process in which the text is sent, as well as the resolutions of Double-Blind Review.

The Editor should evaluate manuscripts and their intellectual content without distinction of race, gender, sexual orientation, religious beliefs, ethnicity, nationality, or the political philosophy of the Authors.

The Editor and his editing team of ECORFAN® Holdings will not disclose any information about Articles submitted to anyone other than the corresponding Author.

The Editor should make fair and impartial decisions and ensure a fair Double-Blind Review.

Responsibilities of the Editorial Board

The description of the peer review processes is made known by the Editorial Board in order that the Authors know what the evaluation criteria are and will always be willing to justify any controversy in the evaluation process. In case of Plagiarism Detection to the Article the Committee notifies the Authors for Violation to the Right of Scientific, Technological and Innovation Authorization.

Responsibilities of the Arbitration Committee

The Arbitrators undertake to notify about any unethical conduct by the Authors and to indicate all the information that may be reason to reject the publication of the Articles. In addition, they must undertake to keep confidential information related to the Articles they evaluate.

Any manuscript received for your arbitration must be treated as confidential, should not be displayed or discussed with other experts, except with the permission of the Editor.

The Arbitrators must be conducted objectively, any personal criticism of the Author is inappropriate.

The Arbitrators must express their points of view with clarity and with valid arguments that contribute to the Scientific, Technological and Innovation of the Author.

The Arbitrators should not evaluate manuscripts in which they have conflicts of interest and have been notified to the Editor before submitting the Article for Double-Blind Review.

Responsibilities of the Authors

Authors must guarantee that their articles are the product of their original work and that the data has been obtained ethically.

Authors must ensure that they have not been previously published or that they are not considered in another serial publication.

Authors must strictly follow the rules for the publication of Defined Articles by the Editorial Board.

The authors have requested that the text in all its forms be an unethical editorial behavior and is unacceptable, consequently, any manuscript that incurs in plagiarism is eliminated and not considered for publication.

Authors should cite publications that have been influential in the nature of the Article submitted to arbitration.

Information services

Indexation - Bases and Repositories

RESEARCH GATE (Germany)
GOOGLE SCHOLAR (Citation indices-Google)
REDIB (Ibero-American Network of Innovation and Scientific Knowledge- CSIC)
MENDELEY (Bibliographic References Manager)
DULCINEA (Spanish scientific journals)
UNIVERSIA (University Library-Madrid)
SHERPA (University of Nottingham - England)

Publishing Services

Citation and Index Identification H
Management of Originality Format and Authorization
Testing Article with PLAGSCAN
Article Evaluation
Certificate of Double-Blind Review
Article Edition
Web layout
Indexing and Repository
ArticleTranslation
Article Publication
Certificate of Article
Service Billing

Editorial Policy and Management

21 Santa Lucía, CP-5220. Libertadores -Sucre – Bolivia. Phones: +52 1 55 6159 2296, +52 1 55 1260 0355, +52 1 55 6034 9181; Email: contact@ecorfan.org www.ecorfan.org

Journal of Experimental Systems

2410 3950
ISSN 2410 - 3950

www.ecorfan.org